A reduction in Drp1 mediated fission compromises mitochondrial health in autosomal recessive spastic ataxia of Charlevoix Saguenay

Teisha Y. Bradshaw[1], Lisa E.L. Romano[1], Emma J. Duncan[1], Suran Nethisinghe[1], Rosella Abeti[3], Gregory J. Michael[2], Paola Giunti[3], Sascha Vermeer[4] and J. Paul Chapple[1]

[1] William Harvey Research Institute, Barts and the London School of Medicine, Queen Mary University of London, London, EC1M 6BQ, United Kingdom.

[2] Blizard Institute, Barts and the London School of Medicine and Dentistry, Queen Mary University of London, London, E1 2AT, United Kingdom.

[3] Department of Molecular Neuroscience, UCL Institute of Neurology, London, WC1N 3BG, United Kingdom.

[4]Department of Clinical Genetics, The Netherlands Cancer Institute, Plesmanlaan 121, 1066 CX Amsterdam, The Netherlands.

Address for correspondence:

Professor Paul Chapple
Centre for Endocrinology
William Harvey Research Institute
Barts and the London School of Medicine
Queen Mary University of London
Charterhouse Square
London EC1M 6BQ
United Kingdom
Tel: +44 20 7882 6242
Email: j.p.chapple@qmul.ac.uk

Abstract

The neurodegenerative disease Autosomal Recessive Spastic Ataxia of Charlevoix Saguenay (ARSACS) is caused by loss of function of sacsin, a modular protein that is required for normal mitochondrial network organisation.

To further understand cellular consequences of loss of sacsin we performed microarray analyses in sacsin knockdown cells and ARSACS patient fibroblasts. This identified altered transcript levels for oxidative phosphorylation and oxidative stress genes. These changes in mitochondrial gene networks were validated by quantitative reverse transcription PCR. Functional impairment of oxidative phosphorylation was then demonstrated by comparison of mitochondria bioenergetics through extracellular flux analyses. Moreover, staining with the mitochondrial specific fluorescent probe MitoSox suggested increased levels of superoxide in patient cells with reduced levels of sacsin.

Key to maintaining mitochondrial health is mitochondrial fission, which facilitates the dynamic exchange of mitochondrial components and separates damaged parts of the mitochondrial network for selective elimination by mitophagy. Fission is dependent on Dynamin related protein 1 (Drp1), which is recruited to prospective sites of division where it mediates scission. In sacsin knockdown cells and ARSACS fibroblasts, we observed a decreased incidence of mitochondrial associated Drp1 foci. This phenotype persists even when fission is induced by drug treatment. Mitochondrial associated Drp1 foci are also smaller in sacsin knockdown cells and ARSACS fibroblasts.

These data suggest a model for ARSACS where neurons with reduced levels of sacsin are compromised in their ability to recruit or retain Drp1 at the mitochondrial membrane leading to a decline in mitochondrial health, potentially through impaired mitochondrial quality control.

Introduction

The neurodegenerative disease Autosomal Recessive Spastic Ataxia of Charlevoix Saguenay (ARSACS: OMIN 270550) was originally identified in Quebec, but is now known to have a worldwide distribution (1, 2). ARSACS is regarded as the second most common recessive ataxia and typically presents with a prominent cerebellar ataxia, spasticity, and peripheral neuropathy. Central to ARSACS pathology is Purkinje cell loss, which has been documented from patient brain and observed in a mouse model of the disease (3-5).

ARSACS is caused by mutations in the *SACS* gene that encodes sacsin/DNAJC29 (1). At 4579 amino acids in length sacsin is one of the largest proteins encoded by the human genome. It is a modular protein that from N- to C-terminus is composed of a ubiquitin-like (UBL) domain that binds to the proteasome (6), three large sacsin repeat regions (SRR) that may have an Hsp90-like chaperone function (7), a J-domain that binds Hsp70 (6, 8) and a higher eukaryotes and prokaryotes nucleotide-binding (HEPN) domain that can dimerise (6-10). Despite the identification of these domains sacsin's cellular role is unknown.

We have previously reported that siRNA mediated knockdown of sacsin leads to a reduction in mitochondrial membrane potential and a more interconnected mitochondrial network in the SH-SY5Y neuroblastoma cell line (3). Mitochondrial membrane potential was also reduced in Purkinje neurons from sacsin knockout mice (3). Subsequently, it has been shown that mitochondria are elongated and have reduced mobility in motor neuron cultures from these KO mice (4), while, in cultured rat hippocampal neurons transduced with lentivirus encoding shRNAmiRs targeting sacsin, mitochondria are clustered and accumulate in the soma and proximal dendrites (3).

There is increasing evidence that perturbation of the equilibrium between mitochondrial fission and fusion underlies mitochondrial defects that contribute to age-related neurodegenerative diseases, including Alzheimer's and Parkinson's (11, 12). This is because mitochondrial dynamics are essential for distribution, traffic and quality control of mitochondria. For mitochondrial quality control fission is required to sequester damaged parts of mitochondrial networks away from healthy mitochondria, acting as a precursor to their degradation by mitophagy (13). Importantly, deficits in mitochondrial fission may be particularly detrimental in neurons as they have bioenergetic demands at sites distant from the cell body requiring that they generate mitochondria of the correct size for transport along dendrites and axons. There is also the possibility that mitochondrial turnover may be restricted to the cell body, as opposed to occurring in axons (14), further linking mitochondrial dynamics and traffic to mitophagy. Moreover, mitochondrial dynamics facilitates the

exchange of mitochondrial matrix and membrane components between individual mitochondrion as part of mitochondrial network maintenance.

As mitochondrial quality control mechanisms are intrinsically linked to mitochondrial division, disruption of fission has potential downstream consequences for important aspects of mitochondrial function. These include impaired oxidative phosphorylation. Unhealthy mitochondria are also likely to accumulate reactive oxygen species (ROS) and other markers of damage. Moreover, there is evidence of reduced mitochondrial fitness in multiple neurodegenerative diseases. For example, in Parkinson's, a disease where the mitochondrial quality control machinery is compromised, respiration is impaired while ROS and antioxidant enzymes increase (15, 16). Evidence supporting impaired bioenergetics in Parkinson's includes that fibroblasts from patients with sporadic disease show a significant decrease in respiration compared to controls (17).

The mechanism through which loss of sacsin impairs mitochondrial function, distribution and network organisation is unclear, but could potentially be explained by either an increase in mitochondrial fusion or a decrease in fission. Supporting a model where loss of sacsin impairs fission we identified, through immunoprecipitation (IP), an interaction between the N-terminal 1368 amino acids of sacsin (encompassing the UBL domain and first SRR) and the dynamin-related GTPase dynamin-related protein 1 (Drp1) (3). During mitochondrial fission Drp1 is recruited from the cytosol onto the outer mitochondrial membrane (OMM), where it assembles into foci. These foci consist of oligomeric Drp1 complexes that are thought to wrap around and constrict the mitochondrial tubule to mediate fission (18).

In this study we used unbiased microarray and gene ontology analyses to identify oxidative phosphorylation and oxidative stress pathways as altered in sacsin knockdown cells and ARSACS patient fibroblasts. Changes in transcript levels for genes in these pathways were confirmed by quantitative reverse transcription PCR (RT-qPCR) in both sacsin knockdown cells and ARSACS patient fibroblasts. Bioenergetics profiles for cells lacking sacsin and accumulation of ROS were also analysed. Using siRNA mediated knockdown and ARSACS patient fibroblast cell lines we also examined the effect of reduced cellular levels of sacsin on Drp1 mitochondrial localisation. We identified a reduction in Drp1 foci at mitochondria and reduced translocation of Drp1 to mitochondria after ablation of mitochondrial membrane potential. This suggests sacsin may play a role in recruitment or retention of Drp1 at mitochondrial fission sites, with loss of this function leading to impaired mitochondrial health.

Results

Microarray analyses implicate altered mitochondrial function in ARSACS

To elucidate pathogenic mechanisms of ARSACS we performed two microarray experiments using a human Illumina Whole Genome Gene Expression BeadChip (HT-12 v4.0). We compared transcript levels in SH-SY5Y cells transfected with siRNAs targeting sacsin and control siRNAs (Figure S1), while in a complimentary experiment, gene expression profiling was performed to compare ARSACS patient and control human dermal fibroblasts (HDFs). For this part of the study four ARSACS HDF lines and two control HDF lines were used. ARSACS HDFS were from three compound heterozygous patients (c.2094-2A>G/Q4054*; K1715*/R4331Q; R2002fs/Q4054*) and one homozygous patient (2801delQ). Immunoblotting of lysates from these ARSACS HDF lines was performed using a commercially available antibody against an undefined sequence between residues 4100 and 4200 of sacsin. This detected a sacsin band in cell homozygous for the single amino acid deletion mutation 2801delQ, which was of similar intensity to that seen in WT control HDFs. In cells with the K1715*/R4331Q mutation a significantly fainter sacsin band was visible. This is consistent with the K1715*/R4331Q HDF line expressing detectable protein from a single allele. No sacsin was detected in the other two ARSACS HDF lines, although we could not preclude expression of a truncated protein (Figure S2). In sacsin knockdown cells 523 genes showed a significant change in expression levels, while in patient cells, expression of 572 genes was altered ($p<0.05$) (Figure 1A). Functional annotation clustering using the Database for Annotation, Visualization and Integrated Discovery (DAVID) (19), identified enrichment of genes in four clusters as common to the microarray comparing SH-SY5Y cells transfected with siRNAs targeting sacsin or scrambled siRNAs and the microarray comparing ARSACS and control HDFs (Figure 1B). Two of these clusters related directly to mitochondria with gene ontology terms including mitochondrial components, cell respiration, oxidative phosphorylation and oxidative stress. From the genes in these groupings we identified 18 genes where transcript levels showed a one fold or greater upregulation or down regulation in both the sacsin knockdown cells (Figure 1C) and ARSACS HDF cells (Figure 1D). These included 10 genes that function in oxidative phosphorylation (*NDUFB3, NDUFB8, NDUFA9, NDUFB9, SDHD, UQCRFS1, COX7B, COX17, ATP5J* and *ATP5J2*), 5 genes linked to oxidative stress (*SOD2, MAFF, FOSB, FOS* and *ATF3*) and 3 genes listed as mitochondrial components (*SUCLA2, MTCH1* and *HSPE1*) (Figure 1D).

Loss of sacsin function causes alterations in levels of oxidative phosphorylation and oxidative stress gene transcripts

To validate alterations in transcript levels of oxidative phosphorylation and oxidative stress genes we used RT-qPCR. In an experiment that was independent from the microarray analyses, total RNA was extracted from sacsin knockdown and control SH-SY5Y cells. RT-qPCR was then

performed for each gene of interest with raw data normalised to *GAPDH* levels. In agreement with the microarray data we observed that expression of 8 oxidative phosphorylation genes were significantly decreased in cells with reduced levels of sacsin (Figure 2A). This included genes in each mitochondrial respiratory chain complex, with *COX17* showing the greatest reduction in transcript levels (>35%). Contrastingly, 2 oxidative stress genes *ATF3* and *FOSB* were slightly increased in sacsin knockdown cells, although these changes were not significant (Figure 2B). *SOD2*, which the microarray suggested was down regulated, was significantly upregulated in sacsin knockdown cells. Moreover, the mitochondrial component genes (*SUCLA2* and *MTCH1*) that were identified as having reduced transcript levels in the microarray experiment were confirmed as being down regulated by RT-qPCR (Figure 2C).

Total RNA was also extracted from the four ARSACS patient HDF cell line and five control HDF lines and RT-qPCR performed. Again we observed a down regulation of oxidative phosphorylation genes (Figure 2D), with 9 of the 10 genes identified from the microarray analyses exhibiting significantly decreased transcript levels in ARSACS HDFs (the exception was *SDHD*). As observed in the knockdown experiment *COX17* was the oxidative phosphorylation gene that showed the greatest reduction in transcript levels (>60%). ARSACS HDFs also exhibited an upregulation of oxidative stress genes (Figure 2E) with *SOD2, ATF3* and *FOSB* transcripts all significantly increased relative to controls. The most dramatic change was for *FOSB*, which showed a more than 150 fold increase in transcript levels. The mitochondrial component genes were also confirmed as down regulated in the patient cells (Figure 2F). With the exception of data for *SOD2*, changes in gene expression identified by the microarray and RT-qPCR experiments were in broad agreement. The combined data from analyses in sacsin knockdown cells and patient HDF demonstrates reduced expression of oxidative phosphorylation genes in cellular models of ARSACS and suggests oxidative stress is increased.

Bioenergetic parameters are altered in sacsin knockdown and ARSACS patient cells.

Bioenergetics profiling was performed to test for functional consequences of altered mitochondrial gene expression in cells lacking sacsin. Oxygen consumption rates (OCR) were measured in SH-SY5Y cells that had previously been transfected with siRNAs targeting sacsin or control siRNAs (Figure 3A). Measurements were made under basal conditions and after sequential treatment with the ATP synthase (complex V) inhibitor oligomycin, followed by the uncoupling agent carbonyl cyanide-*4* (trifluoromethoxy) phenylhydrazone (FCCP). OCR was then determined after mitochondrial respiration was shut down by combined treatment with the complex I inhibitor rotenone and the complex III inhibitor antimycin A. These analyses revealed that basal respiration, ATP production, proton leak, maximal respiration and spare capacity were all reduced in SH-SY5Y cells with reduced levels of sacsin, compared to controls (Figure 3A-B). These key parameters of

mitochondrial respiration where also compared in ARSACS patient HDF and control HDF lines. As observed in SH-SY5Y cells with reduced levels of sacsin, ARSACS patient HDF showed decreased OCR under basal conditions and after addition of mitochondrial inhibitors (Figure 3C-D). Both knockdown cells and HDFs showed a significant reduction in ATP coupled respiration and maximal respiration, strongly suggesting that compromised mitochondrial respiration is a feature of ARSACS.

Increase levels of ROS in ARSACS patient cells.

As gene expression analyses suggested increased oxidative stress in cells with reduced levels of sacsin we performed staining with MitoSOX Red to detect superoxide species. Confocal imaging of HDFs and subsequent measurement of fluorescent intensity revealed increased levels of MitoSOX staining in ARSACS patient cells relative to controls, this was confirmed by quantitative analyses of confocal images (Figure 4). We were unable to validate these findings in sacsin knockdown SH-SY5Y cells, potentially because the transient knockdown did not reduce sacsin levels sufficiently, or for sufficient time, for ROS to accumulate (not shown).

Localisation of Drp1 foci to mitochondria is reduced in sacsin knockdown cells.

The gene expression and functional data presented here support that mitochondrial health is impaired in ARSACS. Potential mechanisms for this could include an increase in the proportion of defective mitochondria in sacsin null cells as a consequence of impaired mitochondrial dynamics and quality control. Moreover, ARSACS associated changes in mitochondrial network organisation are consistent with impaired Drp1 mediated mitochondrial fission (3).

Based on these data we investigated mitochondrial recruitment of Drp1 in sacsin knockdown cells. Here we initially used control HDFs as they have a more distributed mitochondrial network that was better for quantitative imaging of Drp1 association. Cells were transfected with DSRed2-mito along with scrambled siRNAs or siRNAs targeting *SACS*. After 48 hours cells were fixed and stained for Drp1. Firstly, we confirmed that sacsin knockdown in HDFs impacted mitochondrial network organisation, observing that relative to control cells, sacsin knockdown HDFs frequently exhibited a hyperfused mitochondrial phenotype indicated by balloon-like or bulbed mitochondria (Figure S3). Interestingly, we also observed a larger total mitochondrial volume in individual cells transfected with *SACS* siRNAs relative to controls, suggesting increased mitochondrial mass in response to loss of sacsin (Figure S3). We then analysed the number of Drp1 foci localised on individual mitochondria (Figure 5A-B). We observed that for every 1µm along the length of a mitochondrion an average of 0.81±0.047 Drp1 foci occurred. This incidence of mitochondrial associated Drp1 foci was significantly reduced in sacsin knockdown HDFs where only 0.68±0.039 foci localised per 1µm of mitochondrion.

We next tested if this observation reflected a reduction in the capacity of mitochondria in sacsin deficient cells to recruit Drp1 to prospective sites of fission (Figure 5A-B). To induce fission siRNA transfected cells were treated with carbonyl cyanide *m*-chlorophenyl hydrazine (CCCP), which abolishes membrane potential across the inner mitochondrial membrane leading to Drp1 dependent fragmentation of mitochondria and ultimately mitophagy (20). Confocal imaging indicated extensive mitochondrial fragmentation after CCCP treatment in the cells transfected with the scrambled siRNA relative to cells where *SACS* was targeted (Figure 5A). The degree of mitochondria fragmentation was analysed by comparing the number of individual mitochondrion in cells treated with CCCP and vehicle controls. This confirmed that CCCP treatment resulted in higher levels of fragmentation of mitochondrial network in control HDFs than sacsin knockdown cells (Figure S3). Quantitative analyses identified that treatment with CCCP resulted in a significant increase in mitochondrial localized Drp1 foci in scrambled siRNA controls ($p<0.0001$). The number of Drp1 foci at mitochondria also increased in sacsin knockdown cells, but to a lesser degree than for the control (Figure 5B). Moreover, sacsin knockdown cells treated with CCCP still had less mitochondrial localised Drp1 foci than control cells that had not been treated to induce fission. This reduction in Drp1 recruitment was also confirmed in siRNA treated SH-SY5Y cells (Figure S4).

As reduced cellular levels of sacsin impaired Drp1 recruitment to mitochondria we hypothesised the amount of Drp1 in individual foci may also be affected. To investigate this further we measured the diameter of individual cytosolic and mitochondrially localised Drp1 foci in control and sacsin knockdown cells (Figure 5C-D). In control cells we observed that cytosolic Drp1 foci were significantly smaller than those localised to mitochondria ($p<0.0001$), with respective diameters of 0.38±0.0053μm and 0.52±0.0094μm. Comparison of the diameter of Drp1 foci between cells transfected with scrambled and *SACS* siRNA revealed that mitochondrial associated foci were 16% smaller in cells lacking sacsin ($p<0.0001$). In contrast, there was no significant change in the size of cytosolic Drp1 foci between control and sacsin knockdown cells. We also measured the intensity of the Drp1 fluorescent signal for the mitochondrial associated Drp1 foci, observing this was also significantly reduced in sacsin knockdown cells relative to controls ($p<0.01$) (Figure 5E). To further confirm that Drp1 localisation to mitochondria was reduced upon sacsin knockdown we examined levels of the fission factor in mitochondrial fractions generated from SH-SY5Y cells. Immunoblot analyses of total cell lysates and mitochondrial fractions further supported reduced levels of mitochondrial associated Drp1 in cells with reduced levels of sacsin (Figure S4).

A potential explanation for the reduction in mitochondrial associated Drp1 was that total levels of the fission factor are reduced in sacsin knockdown cells. Immunoblot analyses in SH-SY5Y suggested this was not the case, as sacsin knockdown did not significantly alter total Drp1 levels

(Figure 5F and Figure S4). However, when cells transfected with scrambled siRNAs and siRNAs targeting *SACS* were treated with a cross-linking agent before lysates were immunoblotted for Drp1 we observed a reduction in higher molecular weight Drp1 species in sacsin knockdown cells (Figure 5F-G). This may reflect an absence of Drp1:sacsin complexes, but could also indicate that Drp1 higher order oligomers, or complexes between Drp1 and other components of the fission machinery are reduced.

Interestingly, as Drp1-mediated fission may precede removal of damaged mitochondria by mitophagy, we saw some evidence for decreased mitochondrial turnover in sacsin knockdown SH-SY5Y cells. Using the mitochondrial matrix targeted fluorescent protein MitoTimer (21). We cotransfected a Tet-On SH-SY5Y cell line with pTRE-tight-MitoTimer and control siRNAs or siRNAs targeting *SACS*. 24 hours after transfection cells were treated with doxycycline for one hour to induce expression of the MitoTimer protein. A further 24 and 48 hours after this treatment cell were imaged and levels of fluorescence quantified. This showed a significant greater decrease in MitoTimer red fluorescence in control cells relative to sacsin knockdown cells (Figure S5).

Localisation of Drp1 foci to mitochondria is reduced in ARSACS patient fibroblasts

As a precursor to investigating Drp1 recruitment in ARSACS HDFs, we established that altered mitochondrial network morphology was a common feature of all ARSACS patient HDF lines investigated (Figure S6). This was accompanied by an increase in total mitochondrial volume per cell that was significant in two of the ARSACS HDF lines, but not overall (Figure S6). As in sacsin knockdown cells, we quantified the number of Drp1 foci localised on individual mitochondria in patient and control lines. This included a comparison of the number of Drp1 associated mitochondrial foci between vehicle treated cells and cells treated with CCCP to induce unopposed Drp1 recruitment (Figure 6A). We observed that for all the patient cell lines examined, significantly less Drp1 foci were localised to mitochondria than for control cells (Figure 6B and Figure S7). ARSACS patient cells also showed a reduced capacity to increase the number of mitochondrial-associated foci after the induction of fission with CCCP. Mitochondrial associated Drp1 foci were also smaller with a reduced fluorescent intensity (when detected by immunofluorescent staining for Drp1), relative to controls (Figure 6C-D).

In combination, our data in sacsin knockdown cells and ARSACS HDF lines, indicate that loss of sacsin impairs mitochondrial association of Drp1.

Discussion

Data presented here support that decreased mitochondrial function is a feature of ARSACS. Specifically, we show that oxidative phosphorylation is impaired in cells lacking sacsin, including ARSACS patient HDFs. This is also consistent with decreased expression of nuclear genes encoding respiratory chain complex components and other mitochondrial proteins. These observations combined with an increase in expression of oxidative stress gene transcripts demonstrate that mitochondrial health is reduced in ARSACS. This is in agreement with another very recent study that has also reported reduced bioenegetic function and oxidative stress in ARSACS (22). This study compared five patient and control HDFs and did not corroborate findings in any cellular models with isogenic controls (this was a key reason we also performed comparative analyses in sacsin knockdown cells).

Mitochondrial dynamics are disrupted in ARSACS, with our data showing that patient HDFs with a range of different ARSACS mutations have disrupted mitochondrial network organisation. This is consistent with the finding that recruitment of the fission protein Drp1 to the OMM is reduced in both *SACS* knockdown cells and ARSACS patient HDFs. As fission is integral to mitochondrial quality control we hypothesise that a failure to remove damaged mitochondria could explain the reduction in mitochondrial respiration and thus contribute to the molecular pathology of ARSACS. This idea is supported by our observation that mitochondrial turnover, measured by loss of MitoTimer fluorescence after a pulse of expression, is reduced in sacsin knockdown SH-SY5Y cells. In the context of this hypothesis it is important to consider known consequences of impaired Drp1 function. These include that complete loss of Drp1 is embryonic lethal in mice, with fibroblasts from these animals having elongated and more interconnected mitochondria (23, 24). In humans Drp1 also appears to be an essential protein as a mutation at a conserved residue (A359D) in the middle domain of Drp1 was neonatal lethal. In this case fibroblasts again exhibited a phenotype with mitochondrial elongation with tubular structures concentrated around the nucleus (25). Loss of sacsin is not embryonic lethal in mice or humans and Drp1 association with mitochondria is reduced rather than abolished in sacsin null cells. This less severe ARSACS phenotype signifies that sacsin is not essential for Drp1 mediated fission, but may be required for normal regulation of mitochondrial division in some cell types.

This might be more similar to the phenotype in cells depleted for Fis1 and Mff (26). Targeting of these integral OMM proteins, that act as receptors to recruit Drp1 to the mitochondrial surface, were shown to result in increased mitochondrial interconnectivity with a reduction in the number and size of mitochondrial associated Drp1 foci. Despite phenotypic overlap, it seems unlikely that sacsin would function like Fis1 and Mff as a component of the Drp1 receptor machinery. This is

because sacsin is a cytosolic protein that localises at or near the OMM through an unknown mechanism.

Another possible explanation for the decreased association of Drp1 to mitochondria in cells with less sacsin is impaired traffic of Drp1. Modulators of Drp1 distribution include the cytoplasmic dynein machinery, with over expression of the dynactin subunit, dynamitin (p50), altering mitochondrial dynamics and reducing the association of Drp1 with mitochondria (27).

It also seems likely that cytoskeletal disorganisation more broadly contributes to the ARSACS mitochondrial phenotype. Loss of sacsin results in the accumulation of non-phosphorylated neurofilaments in vulnerable neuronal populations in *SACS*$^{-/-}$ mouse and ARSACS patient brain (4). Given that intermediate filaments, actin microfilaments and microtubules form an interlinked cytoskeletal network, it is likely that disruption of neurofilament organisation would impact directly on the distribution of mitochondria and plausibly influence Drp1 dynamics. Interestingly, connections between Drp1 mitochondrial association and cytoskeletal abnormalities have been established in animal models of Alzheimer's disease and related tauopathies. Specifically, mitochondrial elongation as a consequence of Drp1 mislocalisation has been reported in *Drosophila* and mouse neurons expressing human tau, with evidence this is by a mechanism where phosphorylated tau excessively stabilises actin, inhibiting F-actin and myosin dependent translocation of Drp1 and mitochondria, with this contributing to mitochondrial dysfunction and cell death (28).

It is interesting that patient HDFs have detectable cellular phenotypes yet ARSACS is purely a neurodegenerative disease. This supports the hypothesis that abnormal mitochondrial dynamics and function is particularly detrimental to neurons. Explanations of why neurons are highly sensitive to perturbations in mitochondrial dynamics include that they have energy requirements away from the cell body and must be able to traffic mitochondria relatively long distances (12). For ARSACS, impaired traffic is supported by the observation that mitochondrial motility was significantly reduced in axons of *SACS*$^{-/-}$ mouse motor neurons (4). Clues to potential mechanisms of Purkinje cell death, in response to impaired fission, come from studies using mouse postmitotic Purkinje cells depleted for Drp1. In these cells elongated mitochondria ultimately become swollen due to oxidative damage, losing respiratory function and accumulating markers of degradation. Moreover, treatment with antioxidants was shown to be neuroprotective (29). In addition to neurons being particularly vulnerable to aberrant mitochondrial dynamics, they are reported to have very limited glycolysis (30). Relative to some other cell types this makes neurons more highly dependent on aerobic oxidative phosphorylation, which our microarray and bioenergetics data indicates is impaired when sacsin function is lost.

Ultimately, it will be important to analyse the degree of mitochondrial dysfunction associated with ARSACS in neurons. It is encouraging that ARSACS HDFs have robust and quantifiable mitochondrial phenotypes, as this suggests that iPSC derived neurons generated from fibroblasts will be a useful and more disease relevant model.

It has previously been found that oxidative phosphorylation complex assembly and function is modulated by mitochondrial dynamics, including Drp1 mediated fission (31). Moreover, gene expression studies have shown that levels of gene transcripts associated with oxidative phosphorylation, and other aspects of mitochondrial bioenergetics, are often reduced in neurodegenerative disease (32, 33). The expression of nuclear genes involved in mitochondrial function, including those encoding proteins required for oxidative phosphorylation, is controlled by mitochondria-to-nucleus signalling mechanisms. These in turn are modulated by factors such as calcium, ATP and ROS levels (34). It is thus likely that the changes in gene expression observed in response to loss of sacsin are a consequence of the altered mitochondrial dynamics either directly or more indirectly through factors such as the accumulation of ROS.

Although we have shown reduced localisation of Drp1 to the OMM contributes to altered mitochondrial dynamics in ARSACS, the function of sacsin remains unclear. Based on sacsin's repeating structure and large size, one possibility is that it may have a scaffold function. As sacsin has multiple domains that link to molecular chaperone and protein degradation systems it could potentially tether molecules together in a chaperone-regulated system. Alternately, sacsin may function as a chaperone for a specific client or group of client proteins with the possibility that client protein misfolding impacts on Drp1 mediated fission through loss or gain of function. This would be partly analogous to common neurodegenerative diseases where both aberrant protein folding and disrupted mitochondrial dynamics are features.

Materials and Methods

Cell culture and sacsin knockdown

SH-SY5Y cells were from the American Type Culture Collection and were grown in Dulbecco's Minimum Eagle Medium (DMEM) at a 1:1 ratio with Ham's F12 medium. Cells were maintained in medium supplemented with 10% heat-inactivated foetal bovine serum (FCS) containing 100U ml^{-1} penicillin and 100 mg ml-1 streptomycin. ARSACS patient fibroblasts were a gift from Dr Sascha Vermeer and colleagues at Radboud University Nijmegen Medical Centre (Nijmegen, Netherlands). These cells were collected as part of a project approved by the Medical Ethics Committee of the Radboud University (CMO-nr 2014/155). Written informed consent to participate in this study was obtained from all patients. Control human dermal fibroblasts were purchased from PromoCell (Heidelberg, Germany) or were kindly provided by Dr Tristan McKay (Biomedical Sciences, St George's, University of London), or Dr Sascha Vermeer. Control and ARSACS HDF lines used in this work were not closely age or sex matched, but were all between passage 3 and 8. HDFs were cultured in DMEM supplemented with 10% FBS and 50U/ml penicillin and 50µg ml^{-1} streptomycin (final concentration in media 1%). All cells were kept in a constant humidified atmosphere of 5% CO_2 at 37ºC. Cell culture reagents were from Life Technologies (Paisley, UK). To induce mitochondrial fission cells were treated for 1 hour with 20µM CCCP, in their standard culture medium.

For sacsin knockdown a combination of three previously validated siRNAs targeting exons 6 (sense: GGAUGAUCCUCUGAAGGUC), 7 (sense: GCGGCCGAAUUCUAUAAAG) and 9 (sense: CGUAAGAUUUCUAGAUGAC) of *SACS* were used (3, 6). These siRNAs were at a concentration of 10nM each and were transfected in combination using Lipofectamine 3000 (ThermoFisher Scientific, Paisley, Scotland), according to the manufacturers instructions. A negative control siRNA that has no significant sequence similarity to human gene sequences was used as a control at a concentration of 30nM.

Microarrays and RT-qPCR

Total RNA was isolated from SH-SY5Y cells (48 hours post transfection with siRNAs) or from HDFs using the RNeasy Mini kit (Qiagen, Hilden, Germany). RNA samples were then reversed transcribed using the QuantiTect Reverse Transcription Kit (Qiagen) to give cDNA. Gene expression profiling using cDNA from SH-SY5Y or HDFs was then performed using a HumanHT-12 v4 Expression BeadChip arrays (Illumina, San Diego, USA). All arrays were hybridised at 58 °C for 16–20 h, followed by wash and stain procedures according to the Direct Hybridization Assay Guide (Illumina). Fluorescent signals were obtained by scanning with iScan System, and data were extracted with Gene Expression Module 1.0.6 in GenomeStudio Software 2011.1 (Illumina) with or

without background subtraction. Pathway and ontology analysis were performed using DAVID (The Database for Annotation, Visualization and Integrated Discovery) v6.7, which enabled functional annotation clustering (19). RT-qPCR was performed using the MX3000p QPCR Systems (Agilent, Santa Clara, USA). PCR reactions contained 100ng of template cDNA, 200nM of each gene specific primer, 5µl of qPCRBIO SyGreen Mix (PCR Biosystems, London, UK) and were made to a total volume of 10µl with ultra pure water. Relative gene expression was calculated using the 2(-Delta Delta C(T)) ($\Delta\Delta$CT) method where GAPDH was used as the reference gene (35). That GAPDH transcript levels in sacsin knockdown SH-SY5Y cells were not significantly different from controls was confirmed by RT-qPCR using 18S RNA levels for normalisation (not shown). PCR conditions and primer sequence for *NDUFB3, NDUFB8, NDUFA9, NDUFB9, SDHD, UQCRFS1, COX7B, COX17, ATP5J, ATP5J2, SOD2, MAFF, FOSB, FOS, ATF3, SUCLA2, MTCH1, HSPE1* and *GAPDH* are available upon request.

Oxygen consumption rate measurement

Oxygen consumption rate was measured using an XF Extracellular Flux Analyser (Seahorse Bioscience, Massachusetts, USA). SH-SY5Y and HDFs were seeded at densities of 50,000 and 300,000 cells per well respectively. Cells were cultured on Seahorse XF-96 microplates and allowed to grow overnight. On the day of metabolic flux analysis, cells were changed to unbuffered DMEM (DMEM base medium supplemented with 10 mM glucose, 1 mM sodium pyruvate, 2 mM L-Glutamine, pH 7.4) and incubated at 37°C in a non-CO_2 incubator for 1 h. All medium and injection reagents were adjusted to pH 7.4 on the day of assay. Baseline measurements of oxygen consumption rate (OCR, measured by oxygen concentration change) and extracellular acidification rate (ECAR, measured by pH change) were taken before sequential injection of treatments/inhibitors: oligomycin (ATP synthase inhibitor, 4 µM), FCCP (mitochondrial respiration uncoupler, 1 µM), and antimycin A (Complex III inhibitor, 1 µM) in conjunction with rotenone (Complex I inhibitor, 1 µM). Four measurements over time were collected for each condition with 10-12 replicates per sample. Data was normalised to protein concentration (measured by Bradford assay).

Detection of ROS

For detection of ROS cells were seeded in 35mm dishes with a glass insert designed for live cell imaging (MatTek Corporation, Ashland, USA), They were then stained with MitoSOX Red when 80% confluent. For staining, MitoSOX Red was diluted to a final concentration of 5mM solution in phosphate buffer saline (PBS) containing 100 mM calcium and magnesium (PBS/Ca/Mg). Cells were washed once in PBS/Ca/Mg prior to MitoSOX addition and three further times after a 10-minute incubation (at 37ºC in a 5% CO_2 environment) with the dye. For imaging, dishes were placed on a 37°C heated stage and Z-stacks were collected using the 40x objective of a Zeiss

LSM510 laser scanning confocal microscope (Zeiss, Jena, Germany). Fluorescent intensity was measured using the LSM510 Zen software, which allowed for the measurement of fluorescent intensity within a selected region of interest. All confocal image acquisition settings were constant throughout the experiment, including for comparison between patient and control cells.

Immunofluorescent detection and staining

Immunofluorescent staining was as described previously (3). Briefly, cells cultured on glass coverslips were fixed with 4% formaldehyde for 15 minutes and then permeablised for 5 minutes with 0.2% Triton-X 100. Cells were incubated with primary antibodies for 2 hours in 0.02% Triton-X100, 1% bovine serum albumin and 10% normal goat serum, prior to washing and incubation with fluorescently labelled secondary antibodies (Alexa Fluor 488-conjugated goat anti-rabbit or Alexa Fluor 543 conjugated goat anti-mouse (ThermoFisher Scientific). Cells were then counterstained with DAPI and coverslips mounted for microscopy. Primary antibodies were used at the following titres; 1:500 for rabbit polyclonal anti-Tom20 (Santa Cruz Biotechnology); and 1:100 for monoclonal anti-Drp1 (BD Transductions, Oxford, UK). For staining of mitochondria with MitoTracker (ThermoFisher Scientific) the stock solution was diluted to a concentration of 100nM in cell culture media prior to addition to cells for 30 minutes at 37ºC in 5% CO_2 atmosphere. After the incubation period, cells were washed twice cell culture media prior to live imaging or fixation. Confocal microscopy was performed using a LSM510 with a 63x objective.

Morphometric analyses of mitochondrial networks

Morphometric analyses of mitochondrial network organisation was performed on live cells as described previously (3). For volumetric analyses confocal Z-stacks of MitoTracker stained cells were collected and used to generate maximum intensity projections. Surface rendered 3D images generated using the Surpass module of the Imaris image analysis software (Imaris 7.6.1 Bitplane, Concord, USA) were then used to calculate mitochondrial number and volume. Image acquisition settings and thresholding was consistent across datasets.

Quantitative analyses of Drp1 localisation

The number of Drp1 foci per micrometre of mitochondrial length was determined using the line trace function of the LSM510 Zen confocal software. Line trace measured the intensity of channel used for detection of mitochondrial and Drp1 fluorescent staining along individual mitochondria. The number of Drp1 foci along the measured length of mitochondria was then collated from the graphical and tabular output. Drp1 foci intensity and diameter were measured from confocal images using a combination of the Surpass module and MeasurementPro modules of Imaris image analysis software. The mean intensity and diameter of Drp1 was quantified on randomly chosen

mitochondria and in adjacent cytosolic regions in randomly chosen cells from three separate experiments. Area selection was blind to experimental status.

Detection of Drp1 complexes

To study the effect of sacsin knockdown on Drp1 complex formation, SH-SY5Y cells were transfected with either SCRM or SACS siRNA, and 48 hours post-transfection cells were subjected to chemical cross-linking. The cleavable, homo-bifunctional cross-linker dithiobis[succinimidylpropionate] (DSP; Pierce) was added to the cultured cells and incubated for 1 hour at room temperature. Cross-linking was stopped by addition of Tris (pH 7.5) to a final concentration of 20mM. Cells were then lysed and an equal volume of 2x SDS-PAGE sample buffer, without the reducing agent 2-Mercaptoethanol (2-ME). Drp1 was detected with monoclonal anti-Drp1 at a titre of 1:500. GAPDH was also immunoblotted as a loading control with a rabbit anti-GAPDH at a titre of 1:5000 (Abcam).

Mitochondrial turnover

Tet-On SH-SY5Y cells (a gift from Michael Cheetham, University college London), grown on glass coverslips, were co-transfected with pTRE-tight-MitoTimer (21) and control siRNAs or siRNAs targeting *SACS*. 24 hours after transfection cells were transferred to media containing 2μg ml^{-1} doxycycline for our hour. After one hour doxycycline was removed and cells washed before being returned to normal media. Cells were subsequently fixed and prepared for confocal imaging. This was done 24 and 48 hours after the doxycycline pulse. Confocal Z-stacks were collected blind to experimental status and levels of mitochondrial MitoTimer fluorescence analysed from maximum intensity projections. Image acquisition settings and thresholding was consistent across datasets. MitoTimer fluorescent protein has a time-dependent transition from green to red fluorescent emission over time (this has previously been shown to take 48 hours in HEK-293 cells (21)). Consistent with this, and that we achieved a short period of MitoTimer expression, green fluorescence was not at quantifiable levels at 48 hours post the doxacycline treatment in control or sacsin knockdown cells.

Statistical analyses

Statistical significance was determined by a student's t-Test in the sacsin knockdown dataset and ANOVA or Mann-Whitney U tests in the ARSACS patient HDF dataset.

Acknowledgments

This work was supported by BBSRC [BB/L02294X/1]; Fondation de l'Ataxie Charlevoix-Saguenay; and Barts and the London Charity [417/1699].

References

1. Engert, J.C., Berube, P., Mercier, J., Dore, C., Lepage, P., Ge, B., Bouchard, J.P., Mathieu, J., Melancon, S.B., Schalling, M. *et al.* (2000) ARSACS, a spastic ataxia common in northeastern Quebec, is caused by mutations in a new gene encoding an 11.5-kb ORF. *Nat.Genet.*, **24**, 120-125.

2. Vermeer, S., Meijer, R.P., Pijl, B.J., Timmermans, J., Cruysberg, J.R., Bos, M.M., Schelhaas, H.J., van de Warrenburg, B.P., Knoers, N.V., Scheffer, H. *et al.* (2008) ARSACS in the Dutch population: a frequent cause of early-onset cerebellar ataxia. *Neurogenetics*, **9**, 207-214.

3. Girard, M., Lariviere, R., Parfitt, D.A., Deane, E.C., Gaudet, R., Nossova, N., Blondeau, F., Prenosil, G., Vermeulen, E.G., Duchen, M.R. *et al.* (2012) Mitochondrial dysfunction and Purkinje cell loss in autosomal recessive spastic ataxia of Charlevoix-Saguenay (ARSACS). *Proc Natl Acad Sci U S A*, **109**, 1661-1666.

4. Lariviere, R., Gaudet, R., Gentil, B.J., Girard, M., Conte, T.C., Minotti, S., Leclerc-Desaulniers, K., Gehring, K., McKinney, R.A., Shoubridge, E.A. *et al.* (2015) Sacs knockout mice present pathophysiological defects underlying autosomal recessive spastic ataxia of Charlevoix-Saguenay. *Hum Mol Genet*, **24**, 727-739.

5. Bouchard, J.P. (1991) *Recessive spastic ataxia of Charlevoix-Saguenay* Elsevier Science, Amsterdam.

6. Parfitt, D.A., Michael, G.J., Vermeulen, E.G., Prodromou, N.V., Webb, T.R., Gallo, J.M., Cheetham, M.E., Nicoll, W.S., Blatch, G.L. and Chapple, J.P. (2009) The ataxia protein sacsin is a functional co-chaperone that protects against polyglutamine-expanded ataxin-1. *Hum.Mol.Genet.*, **18**, 1556-1565.

7. Anderson, J.F., Siller, E. and Barral, J.M. (2010) The sacsin repeating region (SRR): a novel Hsp90-related supra-domain associated with neurodegeneration. *J Mol Biol*, **400**, 665-674.

8. Anderson, J.F., Siller, E. and Barral, J.M. (2011) The neurodegenerative-disease-related protein sacsin is a molecular chaperone. *J Mol Biol*, **411**, 870-880.

9. Kozlov, G., Denisov, A.Y., Girard, M., Dicaire, M.J., Hamlin, J., McPherson, P.S., Brais, B. and Gehring, K. (2011) Structural basis of defects in the sacsin HEPN domain responsible for autosomal recessive spastic ataxia of Charlevoix-Saguenay (ARSACS). *J Biol Chem*, **286**, 20407-20412.

10. Romano, A., Tessa, A., Barca, A., Fattori, F., de Leva, M.F., Terracciano, A., Storelli, C., Santorelli, F.M. and Verri, T. (2013) Comparative analysis and functional mapping of SACS mutations reveal novel insights into sacsin repeated architecture. *Hum Mutat*, **34**, 525-537.

11. Bereiter-Hahn, J. (2014) Mitochondrial dynamics in aging and disease. *Progress in molecular biology and translational science*, **127**, 93-131.

12. Chen, H. and Chan, D.C. (2009) Mitochondrial dynamics--fusion, fission, movement, and mitophagy--in neurodegenerative diseases. *Hum.Mol.Genet.*, **18**, R169-R176.

13. Lu, B. (2009) Mitochondrial dynamics and neurodegeneration. *Curr Neurol Neurosci Rep*, **9**, 212-219.
14. Devireddy, S., Liu, A., Lampe, T. and Hollenbeck, P.J. (2015) The Organization of Mitochondrial Quality Control and Life Cycle in the Nervous System In Vivo in the Absence of PINK1. *The Journal of neuroscience : the official journal of the Society for Neuroscience*, **35**, 9391-9401.
15. Cassarino, D.S., Fall, C.P., Swerdlow, R.H., Smith, T.S., Halvorsen, E.M., Miller, S.W., Parks, J.P., Parker, W.D., Jr. and Bennett, J.P., Jr. (1997) Elevated reactive oxygen species and antioxidant enzyme activities in animal and cellular models of Parkinson's disease. *Biochim Biophys Acta*, **1362**, 77-86.
16. Yan, M.H., Wang, X. and Zhu, X. (2013) Mitochondrial defects and oxidative stress in Alzheimer disease and Parkinson disease. *Free radical biology & medicine*, **62**, 90-101.
17. Ambrosi, G., Ghezzi, C., Sepe, S., Milanese, C., Payan-Gomez, C., Bombardieri, C.R., Armentero, M.T., Zangaglia, R., Pacchetti, C., Mastroberardino, P.G. *et al.* (2014) Bioenergetic and proteolytic defects in fibroblasts from patients with sporadic Parkinson's disease. *Biochim Biophys Acta*, **1842**, 1385-1394.
18. Mears, J.A., Lackner, L.L., Fang, S., Ingerman, E., Nunnari, J. and Hinshaw, J.E. (2011) Conformational changes in Dnm1 support a contractile mechanism for mitochondrial fission. *Nat Struct Mol Biol*, **18**, 20-26.
19. Huang da, W., Sherman, B.T. and Lempicki, R.A. (2009) Systematic and integrative analysis of large gene lists using DAVID bioinformatics resources. *Nature protocols*, **4**, 44-57.
20. Ishihara, N., Jofuku, A., Eura, Y. and Mihara, K. (2003) Regulation of mitochondrial morphology by membrane potential, and DRP1-dependent division and FZO1-dependent fusion reaction in mammalian cells. *Biochem Biophys Res Commun*, **301**, 891-898.
21. Hernandez, G., Thornton, C., Stotland, A., Lui, D., Sin, J., Ramil, J., Magee, N., Andres, A., Quarato, G., Carreira, R.S. *et al.* (2013) MitoTimer: a novel tool for monitoring mitochondrial turnover. *Autophagy*, **9**, 1852-1861.
22. Criscuolo, C., Procaccini, C., Meschini, M.C., Cianflone, A., Carbone, R., Doccini, S., Devos, D., Nesti, C., Vuillaume, I., Pellegrino, M. *et al.* (2015) Powerhouse failure and oxidative damage in autosomal recessive spastic ataxia of Charlevoix-Saguenay. *J Neurol*, **262**, 2755-2763.
23. Ishihara, N., Nomura, M., Jofuku, A., Kato, H., Suzuki, S.O., Masuda, K., Otera, H., Nakanishi, Y., Nonaka, I., Goto, Y. *et al.* (2009) Mitochondrial fission factor Drp1 is essential for embryonic development and synapse formation in mice. *Nat Cell Biol*, **11**, 958-966.
24. Wakabayashi, J., Zhang, Z., Wakabayashi, N., Tamura, Y., Fukaya, M., Kensler, T.W., Iijima, M. and Sesaki, H. (2009) The dynamin-related GTPase Drp1 is required for embryonic and brain development in mice. *J Cell Biol*, **186**, 805-816.

25. Waterham, H.R., Koster, J., van Roermund, C.W., Mooyer, P.A., Wanders, R.J. and Leonard, J.V. (2007) A lethal defect of mitochondrial and peroxisomal fission. *The New England journal of medicine*, **356**, 1736-1741.

26. Loson, O.C., Song, Z., Chen, H. and Chan, D.C. (2013) Fis1, Mff, MiD49, and MiD51 mediate Drp1 recruitment in mitochondrial fission. *Mol Biol Cell*, **24**, 659-667.

27. Varadi, A., Johnson-Cadwell, L.I., Cirulli, V., Yoon, Y., Allan, V.J. and Rutter, G.A. (2004) Cytoplasmic dynein regulates the subcellular distribution of mitochondria by controlling the recruitment of the fission factor dynamin-related protein-1. *J.Cell Sci.*, **117**, 4389-4400.

28. DuBoff, B., Gotz, J. and Feany, M.B. (2012) Tau promotes neurodegeneration via DRP1 mislocalization in vivo. *Neuron*, **75**, 618-632.

29. Kageyama, Y., Zhang, Z., Roda, R., Fukaya, M., Wakabayashi, J., Wakabayashi, N., Kensler, T.W., Reddy, P.H., Iijima, M. and Sesaki, H. (2012) Mitochondrial division ensures the survival of postmitotic neurons by suppressing oxidative damage. *J Cell Biol*, **197**, 535-551.

30. Parihar, M.S. and Brewer, G.J. (2007) Mitoenergetic failure in Alzheimer disease. *American journal of physiology. Cell physiology*, **292**, C8-23.

31. Liu, W., Acin-Perez, R., Geghman, K.D., Manfredi, G., Lu, B. and Li, C. (2011) Pink1 regulates the oxidative phosphorylation machinery via mitochondrial fission. *Proc Natl Acad Sci U S A*, **108**, 12920-12924.

32. Brooks, W.M., Lynch, P.J., Ingle, C.C., Hatton, A., Emson, P.C., Faull, R.L. and Starkey, M.P. (2007) Gene expression profiles of metabolic enzyme transcripts in Alzheimer's disease. *Brain research*, **1127**, 127-135.

33. Simunovic, F., Yi, M., Wang, Y., Macey, L., Brown, L.T., Krichevsky, A.M., Andersen, S.L., Stephens, R.M., Benes, F.M. and Sonntag, K.C. (2009) Gene expression profiling of substantia nigra dopamine neurons: further insights into Parkinson's disease pathology. *Brain : a journal of neurology*, **132**, 1795-1809.

34. Reinecke, F., Smeitink, J.A. and van der Westhuizen, F.H. (2009) OXPHOS gene expression and control in mitochondrial disorders. *Biochim Biophys Acta*, **1792**, 1113-1121.

35. Livak, K.J. and Schmittgen, T.D. (2001) Analysis of relative gene expression data using real-time quantitative PCR and the 2(-Delta Delta C(T)) Method. *Methods*, **25**, 402-408.

Figure Legends

Figure 1. Microarray analyses identify altered expression of genes associated with mitochondrial function in cells with reduced levels of sacsin. (A) Schematic summary of microarray study design. Two microarray experiments were performed. The first compared gene expression in SH-SY5Y cells transfected with siRNAs targeting sacsin (*SACS*) and scrambled (*SCRM*) control siRNAs. The second experiment compared gene expression in ARSACS patient and WT control HDF. Gene ontology analyses were used to identify functional clusters of genes that were altered in both experiments. **(B)** Functional clustering of mitochondrial genes identified as having altered expression by microarray analyses in both *SACS* knockdown SH-SY5Y and ARSACS patient HDFs. **(C)** Fold change in expression of mitochondrial genes identified through microarray analyses comparing SH-SY5Y cells transfected with siRNAs targeting sacsin and scrambled siRNAs. **(D)** Fold change in expression of mitochondrial genes identified through microarray analyses comparing ARSACS patient and WT control HDFs.

Figure 2. RT-qPCR analyses shows cells with reduced levels of sacsin have alterations in levels of oxidative phosphorylation and oxidative stress gene transcripts. Comparison of transcript levels of oxidative phosphorylation **(A)**, oxidative stress **(B)**, and mitochondrion component **(C)** genes between SH-SY5Y cells transfected with siRNAs targeting sacsin and scrambled siRNAs. RT-qPCR was performed on total RNA extracted from 5 separate knockdown *SACS* experiments. Transcript levels of the genes analysed were normalised to GAPDH levels with data shown as mean fold change relative to cells transfected with scrambled siRNA (*SCRM*). Statistical significances determined by t-test are indicated. Comparison of transcript levels of oxidative phosphorylation **(D)**, oxidative stress **(E)**, and mitochondrion component **(F)** genes between ARSACS patient and WT control HDFs. RT-qPCR was performed on total RNA extracted from 4 ARSACS HDF lines and 5 WT control HDF lines. Transcript levels of the genes analysed were normalised to GAPDH levels with data shown as mean fold change relative to WT controls. Statistical significances were determined by Mann-Whitney U test. Error bars = SD. * $p \leq 0.05$, ** $p \leq 0.005$, *** $p \leq 0.005$.

Figure 3. Bioenergetic function of mitochondria is impaired in sacsin knockdown and ARSACS patient cells. (A) Comparison of oxygen consumption rate (OCR) between cells transfected with siRNAs targeting sacsin and control siRNAs. **(B)** Comparison of basal respiration, ATP production, proton leak, maximum respiration and spare capacity in cells transfected with siRNAs targeting sacsin and control siRNAs, were calculated from the mean of 4 time points **(C)** Comparison of OCR between ARSACS patient and control cell lines. Measurements were made under basal conditions and after addition of oligomycin, FCCP and Antimycin A plus rotenone

(arrows indicate the time points when drugs were added). **(D)** Comparison of basal respiration, ATP production, proton leak, maximum respiration and spare capacity in ARSACS patient and control HDFs, were calculated from the mean of 4 time points. For siRNA knockdown experiments n=12 (12 independent transfection for *SACS* and *SCRM* siRNAs) and for ARSACS patient cells n=4 (4 patient and 4 control HDF lines). Statistical significances were determined by T test or Mann-Whitney U test as appropriate. Error bars = SD. * p≤0.05, ** p≤0.005, *** p≤0.005.

Figure 4. Levels of ROS are increased in ARSACS patient HDFs relative to controls. (A) Representative images of wild-type control and ARSACS patient HDFs stained the mitochondrial superoxide indicator MitoSOX (red). Live cell confocal imaging was used to generate maximum intensity projections. Scale bar = 10μm **(B)** MitoSOX fluorescent intensity was then quantified in individual cells from confocal maximum intensity projections (measurements were made in 25 cells in each patient and control line with three experimental replicates). Error bars = SEM. * p≤0.05, ** p≤0.005, *** p≤0.005.

Figure 5. Localisation of Drp1 to mitochondria is reduced in sacsin knockdown cells. (A) HDFs were cotransfected with control scrambled (*SCRM*) siRNA or siRNA targeting sacsin (*SACS*) and DSRed2-mito (red). After 48 hours cells were treated for 1 hour with 20 CCCP and then processed for immunofluorescent detection of Drp1 (green) and counterstained with DAPI (blue) for nuclei. Examples of mitochondrial associated Drp1 foci are indicated by arrows. Scale bar = 10μm **(B)** The number of Drp1 foci that localised to mitochondria in *SCRM* and *SACS* cells with and without CCCP treatment were then quantified from confocal *Z*-stacks. This data was expressed as the number of Drp1 foci localised to mitochondria per 1 μm of measured length (quantification was performed from at least 6 mitochondria in 60 cells for each treatment, from three independent replicates). **(C)** Panel showing representative micrographs used to quantify the diameter **(D)** and fluorescent intensity **(E)** of mitochondrial associated and cytosolic localised Drp1 foci (at least 450 foci were measured from 18 cells, from 3 independent replicates). **(F)** Immunoblot showing high molecular weight Drp1 complexes are reduced in sacsin knockdown cells. SH-SY5Y cells were transfected with control scrambled (*SCRM*) siRNA or siRNA targeting sacsin (*SACS*). After 48 hours cells were treated with the crosslinker DSP and lysed. Total cell lysates were blotted under reducing (+2-ME) and non-reducing conditions for Drp1. Levels of sacsin in SCRM and SACS cells were assessed by immunoblot for sacsin while GAPDH was used as a loading control. Arrow indicates high molecular weight Drp1 species. (G) Densitometry analyses of immunoblots was used to quantify the ratio of high molecular weight Drp1 complexes relative to monomeric Drp1 (n=5). Statistical significances were determined by T test. Error bars = SEM. * p≤0.05, ** p≤0.005, *** p≤0.005.

Figure 6. Localisation of Drp1 to mitochondria is reduced in ARSACS patient cells. (A) Control and patient HDFs were treated for 1 hour with CCCP and then processed for immunofluorescent detection of Tom20 (red) and Drp1 (green). Cells were also counterstained with DAPI (blue) to detect nuclei. Representative images are shown for two control lines (WT1 and WT2) and each ARSACS patient line used in this study. Examples of mitochondrial associated Drp1 foci are indicated by arrows. Scale bar = 10μm. **(B)** The number of Drp1 foci that localised to mitochondria in control and patient HDFs with and without CCCP treatment were then quantified from confocal *Z*-stacks. This data was expressed as the number of Drp1 foci localised to mitochondria per 1 μm of measured length (using 4 patient and 4 control lines quantification was performed from at least 6 mitochondria in 45 cells for each treatment, from three independent replicates). **(C-D)** Quantification of the diameter (C) and fluorescent intensity (D) of mitochondrial associated and cytosolic localised Drp1 foci (at least 500 foci were measured from 18 cells, from 3 independent replicates). Statistical significances were determined by Mann-Whitney U test. Error bars = SEM. * $p \leq 0.05$, ** $p \leq 0.005$, *** $p \leq 0.005$.

Supplementary: Figure Legends

Figure S1. Confirmation of efficient siRNA-mediated knockdown of sacsin. (A) SH-SY5Ys were cotransfected with control scrambled (*SCRM*) siRNA or siRNA targeting sacsin (*SACS*) and DSRed2-mito (red). After 48 hours cells were stained for sacsin (green) and confocal imaging performed. The siRNAs were in excess to the DSRed2-mito plasmid in the transfection (molar ratio 168,000:1), such that we assumed any cell expressing DSRed2-mito would also contain the siRNAs. Confocal imaging demonstrated sacsin staining (indicated by arrows) was reduced in transfected cells. **(B)** Cell lysates were also generated from scrambled siRNA and sacsin siRNA transfected cells with levels of knockdown assessed by immunoblotting. β-actin used as a loading control. **(C)** Quantitative analyses by densitometry indicated that 48 hours post transfection cellular levels of sacsin were reduced by more than 80%. The anti-sacsin used was a commercial antibody that binds an unknown peptide between residues 4100 and 4200 of human sacsin.

Figure S2. Phenotype of ARSACS HDF cell lines used in this study. (A) Summary of phenotypic characteristics of ARSACS patients who provided HDFs for this study. All patients were clinically examined by a neurologist using the Scale for the Assessment and Rating of Ataxia (SARA). This is an eight item scale that provides a comprehensive rating of simple ataxia tests including the following items: gait, stance, sitting, speech disturbance, finger chase, nose-finger test, fast alternating movements and heel-shin slide. All patients showed severe gait spasticity. All patients displayed severe lower limb spasticity except for patient 3 who showed moderate lower limb spasticity but with a mild upper limb spasticity that was not seen in the other 3 patients. They all displayed a sensomotor axonal neuropathy on EMG, with a secondary demyelination occurring in patient 4. **(B)** Immunoblot analyses of lysates from four WT control and four ARSACS HDF cell lines. Patient numbers correspond with those in the table (A). Lysates were also probed with β-actin as a loading control. Error bars = SD

Figure S3. Sacsin knockdown HDFs have a hyperfused phenotype. (A) HDFs were cotransfected with control scrambled (*SCRM*) siRNA or siRNA targeting sacsin (*SACS*) and DSRed2-mito (red). Confocal imaging was then performed, with representative images shown. Scale bar = 10μm. **(B)** Incidence of cells containing hyperfused mitochondria was then quantified blind to experimental status. **(C)** Surface rendered 3D images were generated from confocal Z-stacks of HDF and used to calculate the mean mitochondrial volume per cell in control transfected and sacsin knockdown cells. **(D)** The number of individual mitochondrion was also quantified in control transfected and sacsin knockdown cells, after 1 hour treatment with vehicle control or 20μM CCCP to induce mitochondrial fission. Statistical significances were determined by T test. Error bars = SD.

Figure S4. Localisation of Drp1 to mitochondria is reduced in sacsin knockdown SH-SY5Y cells. (A) SH-SY5Ys were cotransfected with control scrambled (SCRM) siRNA or siRNA targeting sacsin (SACS) and DSRed2-mito (red). After 48 hours cells were treated for 1 hour with CCCP and then processed for immunofluorescent detection of Drp1 (green) and counterstained with DAPI (blue) for nuclei. Examples of mitochondrial associated Drp1 foci are indicated by arrows. Scale bar = 10μm. **(B)** The number of Drp1 foci that localised to mitochondria in SCRM and SACS cells with and without CCCP treatment were then quantified from confocal Z-stacks. This data was expressed as the number of Drp1 foci localised to mitochondria per 1 μm of measured length (quantification was performed from at 14 cells per treatment, from three independent replicates). Statistical significances were determined by T test. Error bars = SEM. ** p≤0.001, *** p≤0.005. **(C)** Levels of Drp1 in SCRM and SACS cells were assessed by immunoblot, while GAPDH was used as a loading control. **(D)** Quantitative analyses by densitometry indicated that 48 hours post transfection total cellular levels of Drp1 were not significantly altered in sacsin knockdown cells. **(E)** Representative immunoblot of SH-SY5Y cells transiently transfected with *SACS* or *SCRM* siRNA and subjected to subcellular fractionation. Total (T) and mitochondrial (M) fractions were immunoblotted for Drp1 and Tom20. **(F)** Densitometric analysis of DRP1 levels in the mitochondrial fraction relative to TOM20 suggests a reduction in *SACS* compared to *SCRM* siRNA treated cells (n = 2). Error bars = SD (in D and F)

Figure S5. Mitochondrial turnover is decreased in sacsin knockdown cells. (A) Representative images of SH-SY5Y cells 24 and 48 hours after a pulse of MitoTimer protein expression. Tet-On SH-SY5Y were cotransfected with control scrambled (*SCRM*) siRNA or siRNA targeting sacsin (*SACS*) and pTRE-tight-MitoTimer (red). After 24 hours cells were treated for 1 hour with doxycycline and then returned to normal media for a further 24 or 48 hours prior to fixation and confocal imaging. **(B)** MitoTimer red fluorescent intensity was then quantified in individual cells from confocal maximum intensity projections (data is from a representative experiment, where a minimum of 9 cells was imaged per condition). MitoTimer green fluorescence was not at quantifiable levels at 48 hours post the doxacycline treatment in control or sacsin knockdown cells, consistent with a short period of MitoTimer expression, and is not shown. Error bars = SEM. ** p≤0.005.

Figure S6. Mitochondrial network organisation is altered in ARSACS patient HDFS. (A) Confocal Z-stacks of live control and patient HDFs stained with MitoTraker were acquired to generate maximum intensity projections. Scale bar = 10μm **(B)** Surface rendered 3D images were generated from this data and used to calculate the number of individual mitochondria and their volume. This data is shown as the frequency of individual mitochondria for a representative control cell line and each patient analysed. **(C-D)** From these data the average mitochondrial volume per

cell (in μm^3) was calculated. This is shown for each patient cell line (C) and cumulative for the 4 patient cells lines analysed (D). Measurements were made in at least 25 cells per line. Error bars = SEM.

Figure S7. Localisation of Drp1 to mitochondria is reduced in all ARSACS patient cell lines. (A) Control and patient HDFs were treated for 1 hour with CCCP and then processed for immunofluorescent detection of mitochondria and Drp1. The number of Drp1 foci that localized to mitochondria in control and patient HDFs with and without CCCP treatment were then quantified from confocal Z-stacks. This is shown for individual patient cell lines. This data was expressed as the number of Drp1 foci localized to mitochondria per 1 µm of measured length (quantification was performed from at least 6 mitochondria in 45 cells for each treatment, from three independent replicates). Error bars = SEM. *** $p \leq 0.005$.

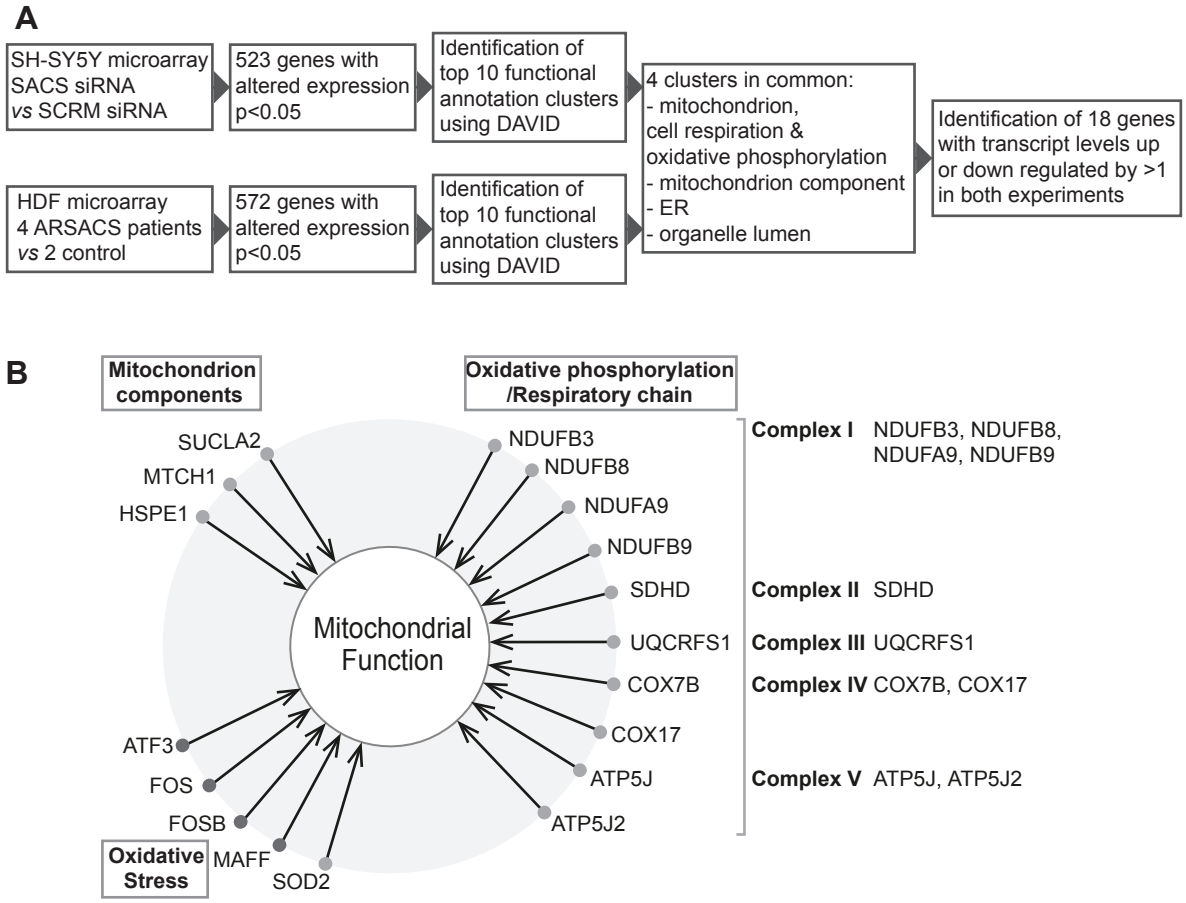
A
SH-SY5Y microarray SACS siRNA vs SCRM siRNA
523 genes with altered expression p<0.05
Identification of top 10 functional annotation clusters using DAVID
HDF microarray 4 ARSACS patients vs 2 control
572 genes with altered expression p<0.05
Identification of top 10 functional annotation clusters using DAVID
4 clusters in common:
- mitochondrion,
cell respiration &
oxidative phosphorylation
- mitochondrion component
- ER
- organelle lumen
Identification of 18 genes with transcript levels up or down regulated by >1 in both experiments
B
Mitochondrion components
Oxidative phosphorylation /Respiratory chain
SUCLA2
MTCH1
HSPE1
NDUFB3
NDUFB8
NDUFA9
NDUFB9
SDHD
UQCRFS1
COX7B
COX17
ATP5J
ATP5J2
Mitochondrial Function
ATF3
FOS
FOSB
MAFF
SOD2
Oxidative Stress
Complex I NDUFB3, NDUFB8, NDUFA9, NDUFB9
Complex II SDHD
Complex III UQCRFS1
Complex IV COX7B, COX17
Complex V ATP5J, ATP5J2
C
SACS KD vs SCRM
NDUFB3
NDUFB8
NDUFA9
NDUFB9
SDHD
UQCRFS1
COX7B
COX17
ATP5J
ATP5J2
SUCLA2
MTCH1
HSPE1
SOD2
ATF3
FOS
FOSB
MAFF
-2 -1 0 1 2
Fold change
D
ARSACS Patient vs CON
NDUFB3
NDUFB8
NDUFA9
NDUFB9
SDHD
UQCRFS1
COX7B
COX17
ATP5J
ATP5J2
SUCLA2
MTCH1
HSPE1
SOD2
ATF3
FOS
FOSB
MAFF
-3 -2 -1 0 1 2 3 4 5 6 7 8 9
Fold change

Figure 1

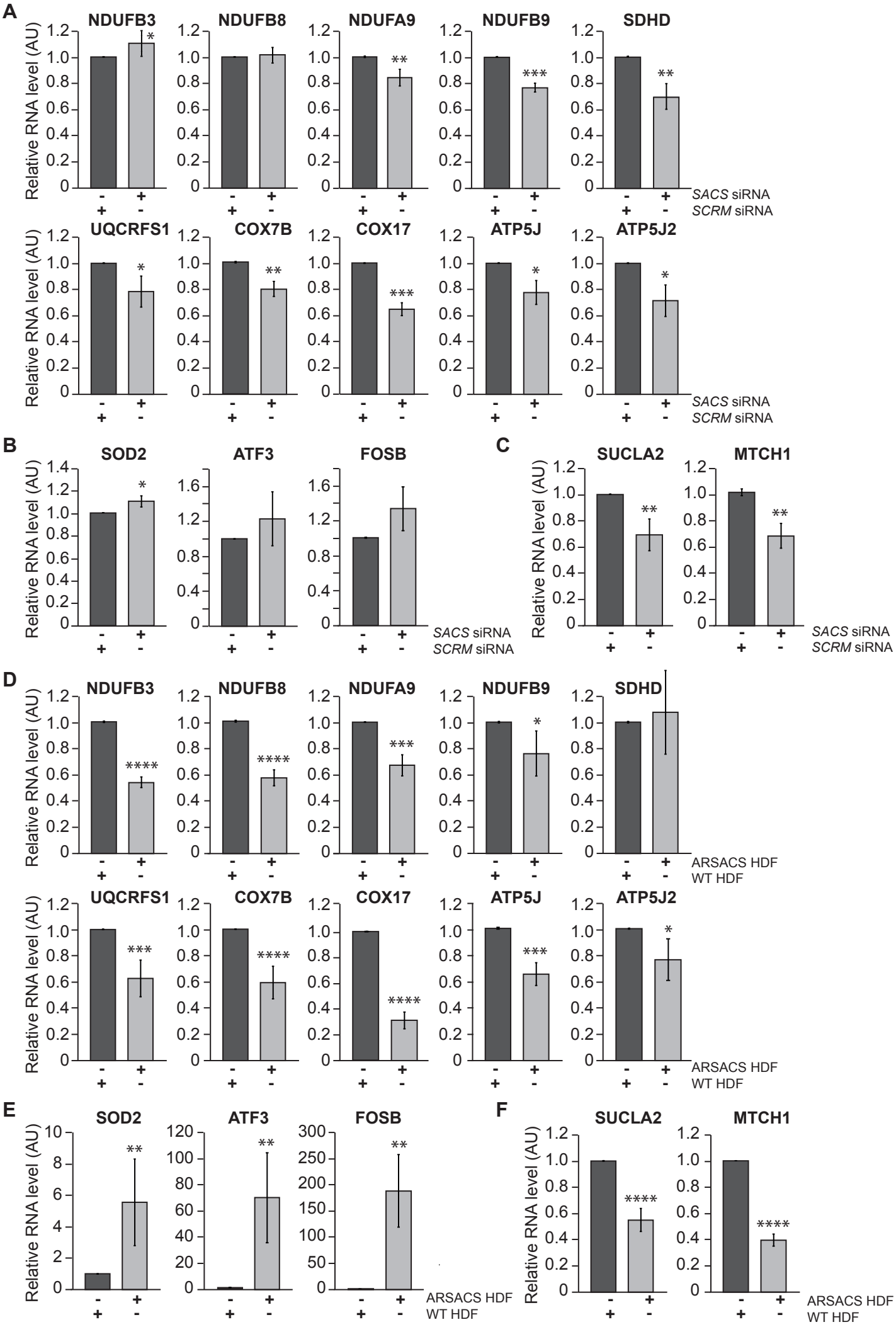
A
NDUFB3
NDUFB8
NDUFA9
NDUFB9
SDHD
UQCRFS1
COX7B
COX17
ATP5J
ATP5J2
Relative RNA level (AU)
SACS siRNA
SCRM siRNA
B
SOD2
ATF3
FOSB
C
SUCLA2
MTCH1
D
ARSACS HDF
WT HDF
E
F

Figure 2

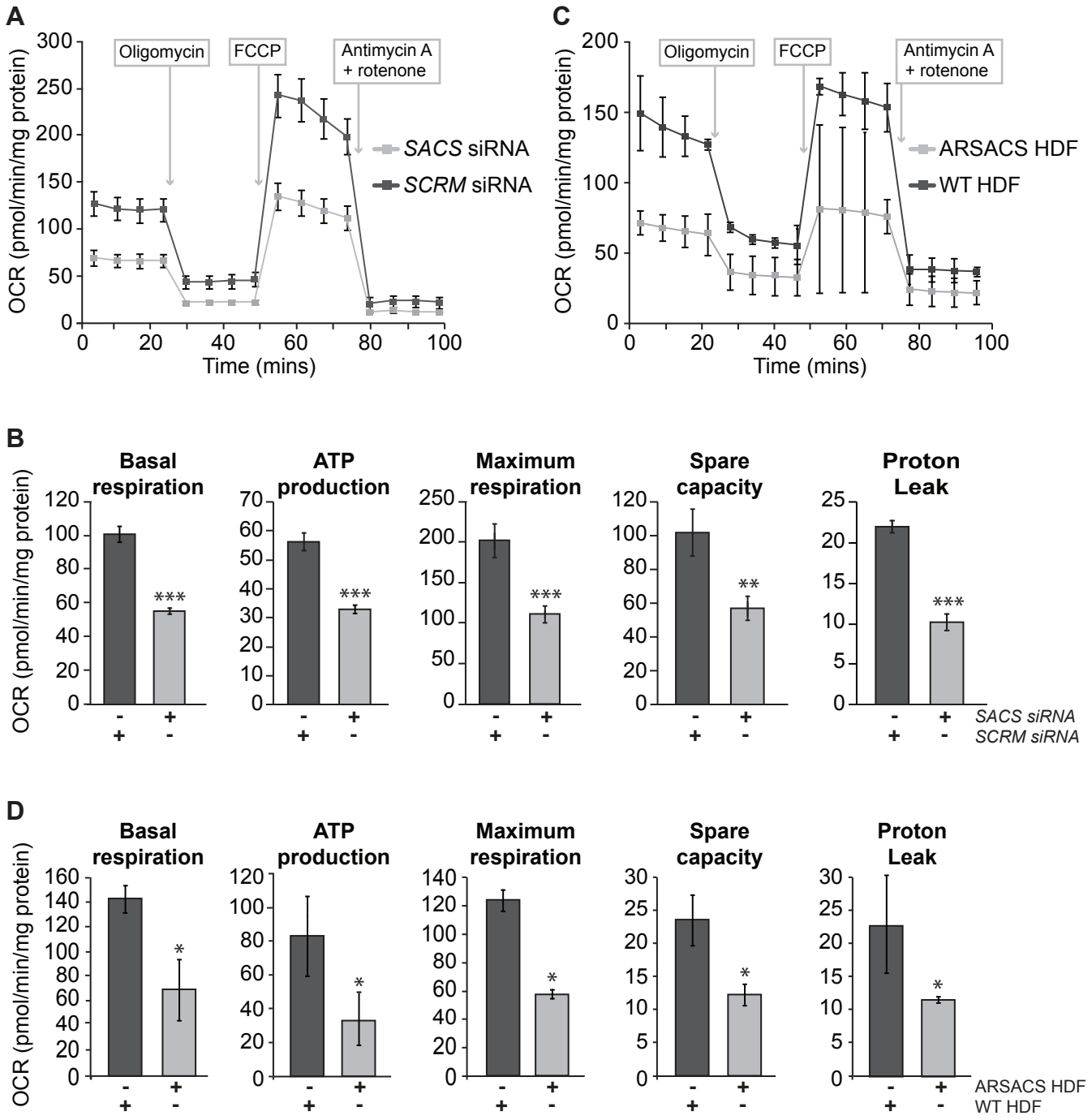
A
Oligomycin
FCCP
Antimycin A + rotenone
OCR (pmol/min/mg protein)
Time (mins)
SACS siRNA
SCRM siRNA
C
ARSACS HDF
WT HDF
B
Basal respiration
ATP production
Maximum respiration
Spare capacity
Proton Leak
D

Figure 3

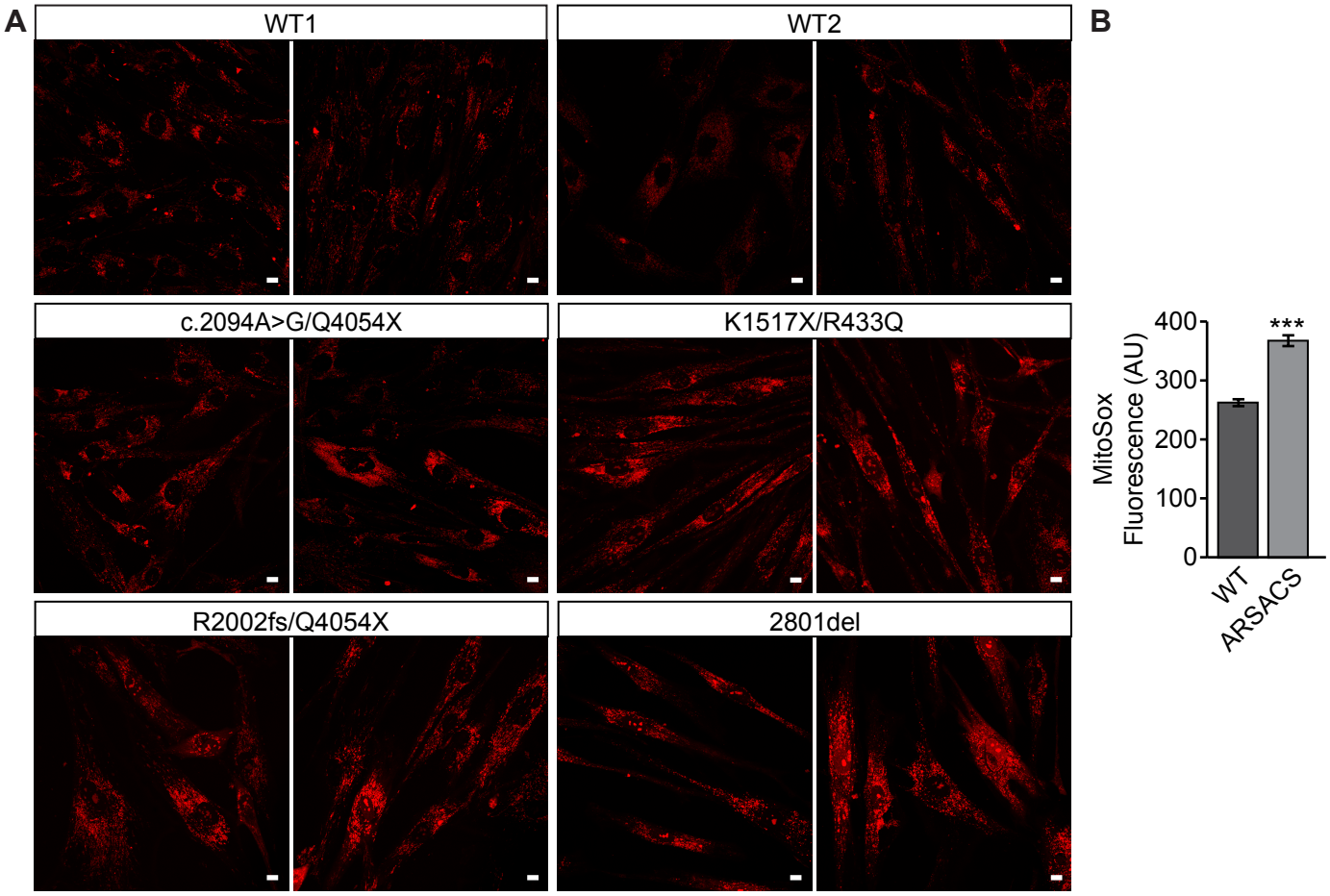
A
WT1
WT2
c.2094A>G/Q4054X
K1517X/R433Q
R2002fs/Q4054X
2801del
B
MitoSox Fluorescence (AU)
400
300
200
100
0
***
WT
ARSACS

Figure 4

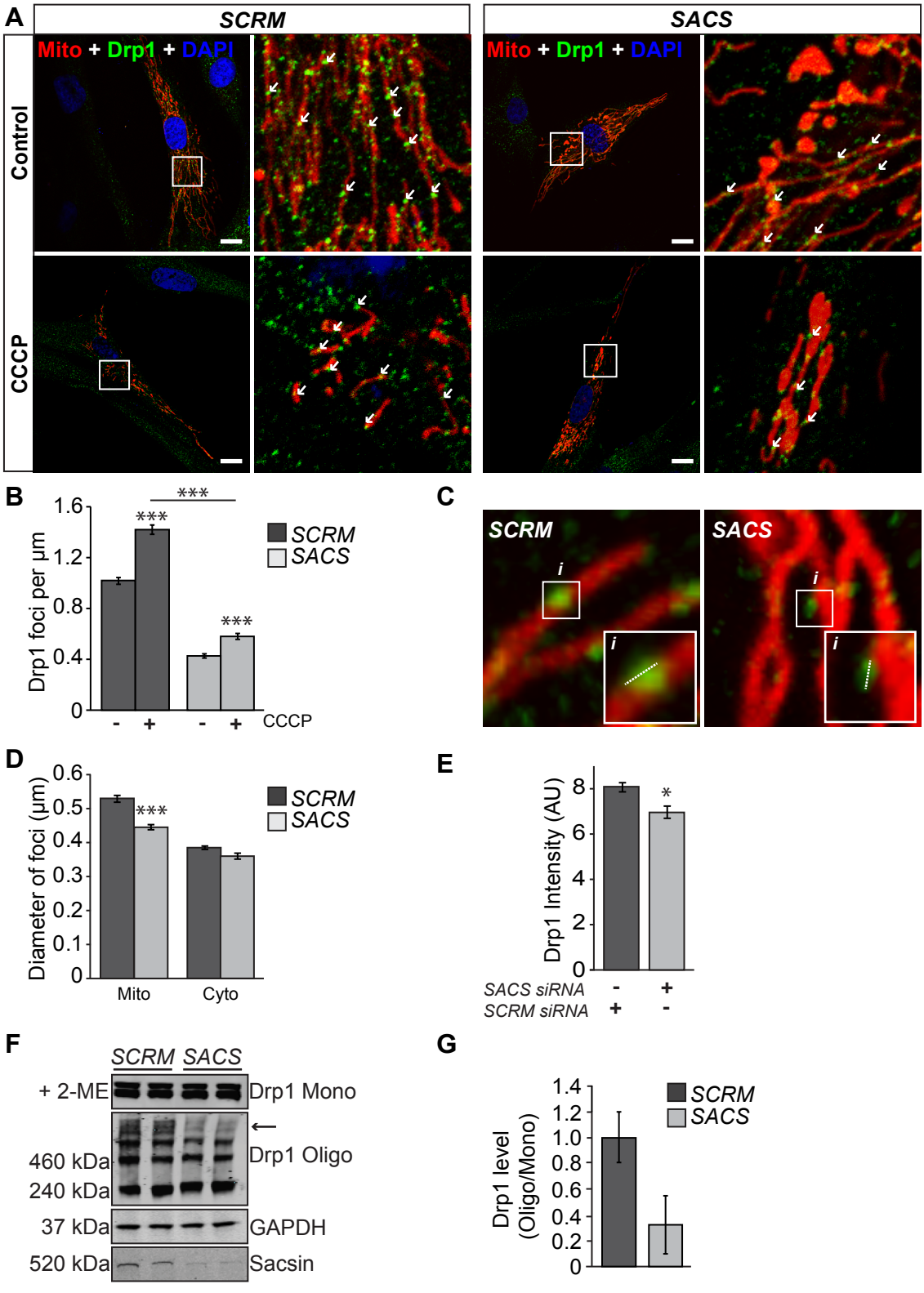
A
SCRM
SACS
Mito + Drp1 + DAPI
Control
CCCP
B
Drp1 foci per µm
SCRM
SACS
CCCP
C
i
D
Diameter of foci (µm)
Mito
Cyto
E
Drp1 Intensity (AU)
SACS siRNA
SCRM siRNA
F
+ 2-ME
Drp1 Mono
Drp1 Oligo
460 kDa
240 kDa
37 kDa
GAPDH
520 kDa
Sacsin
G
Drp1 level (Oligo/Mono)

Figure 5

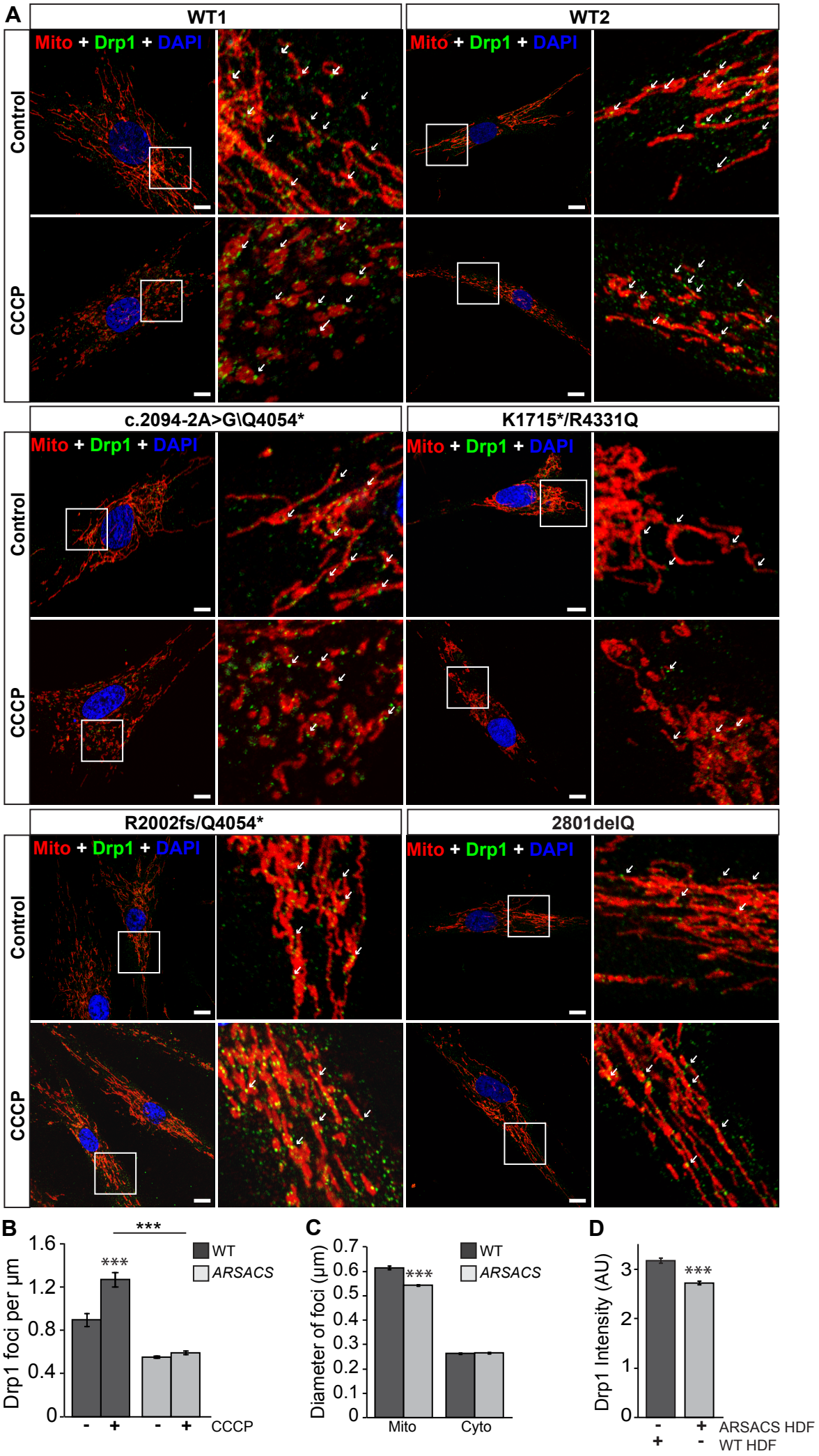
A
WT1
WT2
c.2094-2A>G\Q4054*
K1715*/R4331Q
R2002fs/Q4054*
2801delQ
Mito + Drp1 + DAPI
Control
CCCP
B
Drp1 foci per µm
WT
ARSACS
***
CCCP
C
Diameter of foci (µm)
Mito
Cyto
D
Drp1 Intensity (AU)
ARSACS HDF
WT HDF

Figure 6

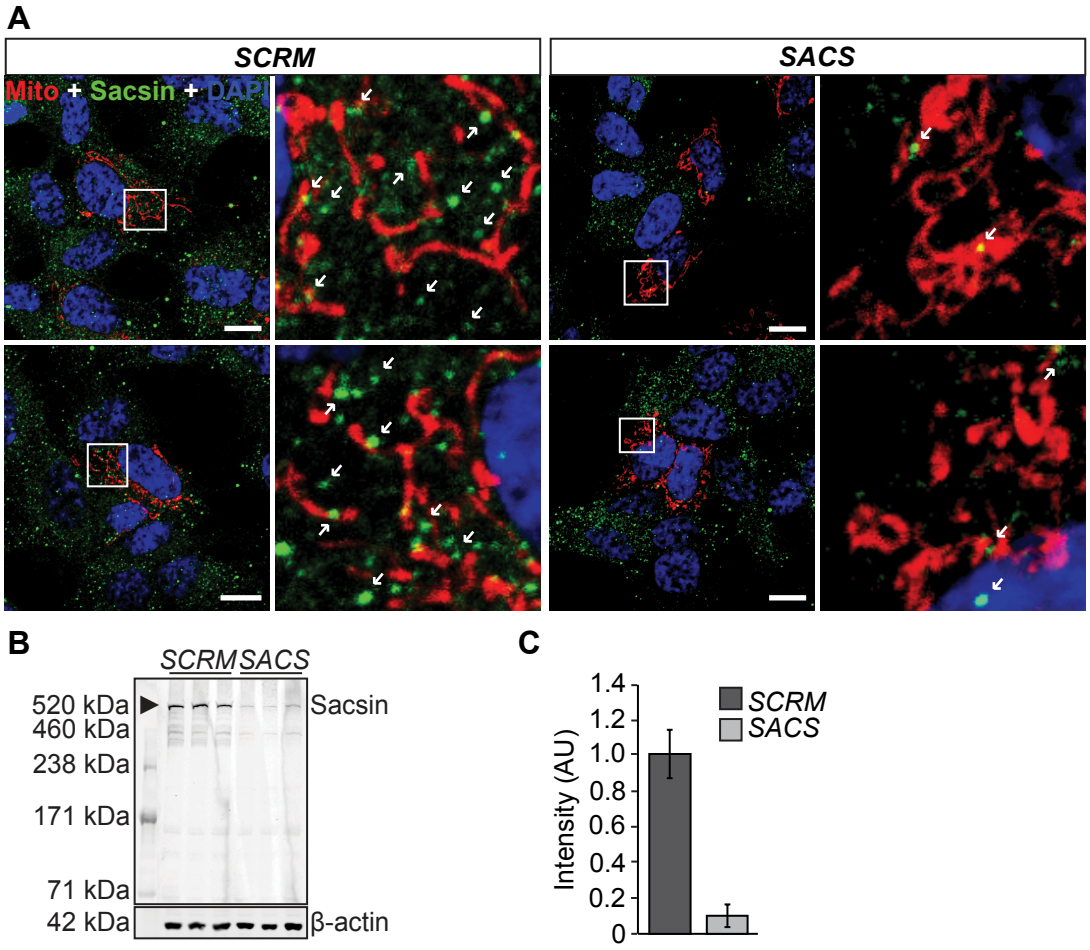

Figure S1. Confirmation of efficient siRNA-mediated knockdown of sacsin. (A) SH-SY5Ys were cotransfected with control scrambled (*SCRM*) siRNA or siRNA targeting sacsin (*SACS*) and DSRed2-mito (red). After 48 hours cells were stained for sacsin (green) and confocal imaging performed. The siRNAs were in excess to the DSRed2-mito plasmid in the transfection (molar ratio 168,000:1), such that we assumed any cell expressing DSRed2-mito would also contain the siRNAs. Confocal imaging demonstrated sacsin staining (indicated by arrows) was reduced in transfected cells. **(B)** Cell lysates were also generated from scrambled siRNA and sacsin siRNA transfected cells with levels of knockdown assessed by immunoblotting. β-actin used as a loading control. **(C)** Quantitative analyses by densitometry indicated that 48 hours post transfection cellular levels of sacsin were reduced by more than 80%. The anti-sacsin used was a commercial antibody that binds an unknown peptide between residues 4100 and 4200 of human sacsin.

A

ARSACS patient	Age at onset (yrs)	Disease duration (yrs)	Disease stage	SARA total score (0-40)	*SACS* mutations	Type of mutation
1	1	39	3	23.5	Q4054* & c.2094-2A>G	Nonsense/Splice-site
2	3	33	3	23	R2002fs & Q4054*	Frameshift/Nonsense
3	1	25	3	19.5	p.2801delQ	In frame deletion
4	8	45	3	21	K1715* & R4331Q	Nonsense/Missense

B

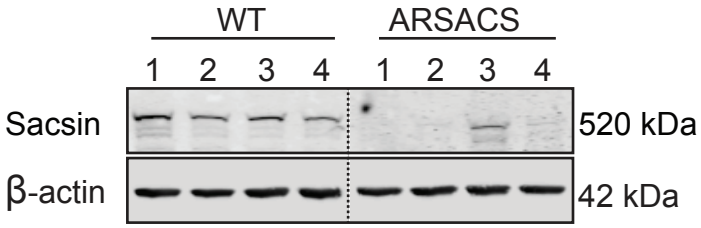

Figure S2. Phenotype of ARSACS HDF cell lines used in this study. (A) Summary of phenotypic characteristics of ARSACS patients who provided HDFs for this study. All patients were clinically examined by a neurologist using the Scale for the Assessment and Rating of Ataxia (SARA). This is an eight item scale that provides a comprehensive rating of simple ataxia tests including the following items: gait, stance, sitting, speech disturbance, finger chase, nose-finger test, fast alternating movements and heel-shin slide. All patients showed severe gait spasticity. All patients displayed severe lower limb spasticity except for patient 3 who showed moderate lower limb spasticity but with a mild upper limb spasticity that was not seen in the other 3 patients. They all displayed a sensomotor axonal neuropathy on EMG, with a secondary demyelination occurring in patient 4. **(B)** Immunoblot analyses of lysates from four WT control and four ARSACS HDF cell lines. Patient numbers correspond with those in the table (A). Lysates were also probed with β-actin as a loading control. Error bars = SD

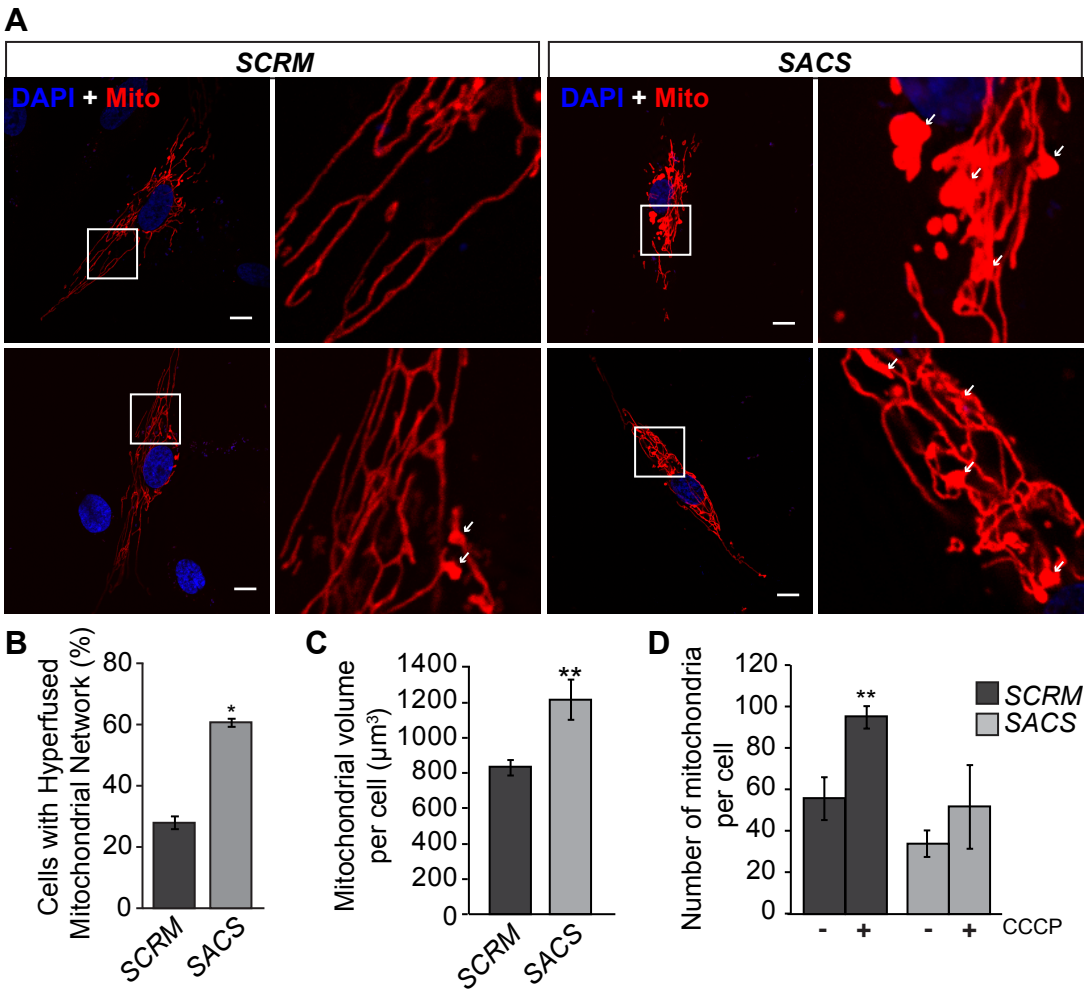

Figure S3. Sacsin knockdown HDFs have a hyperfused phenotype. (A) HDFs were cotransfected with control scrambled (*SCRM*) siRNA or siRNA targeting sacsin (*SACS*) and DSRed2-mito (red). Confocal imaging was then performed, with representative images shown. Scale bar = 10μm. **(B)** Incidence of cells containing hyperfused mitochondria was then quantified blind to experimental status. **(C)** Surface rendered 3D images were generated from confocal Z-stacks of HDF and used to calculate the mean mitochondrial volume per cell in control transfected and sacsin knockdown cells. **(D)** The number of individual mitochondrion was also quantified in control transfected and sacsin knockdown cells, after 1 hour treatment with vehicle control or 20μM CCCP to induce mitochondrial fission. Statistical significances were determined by T test. Error bars = SD.

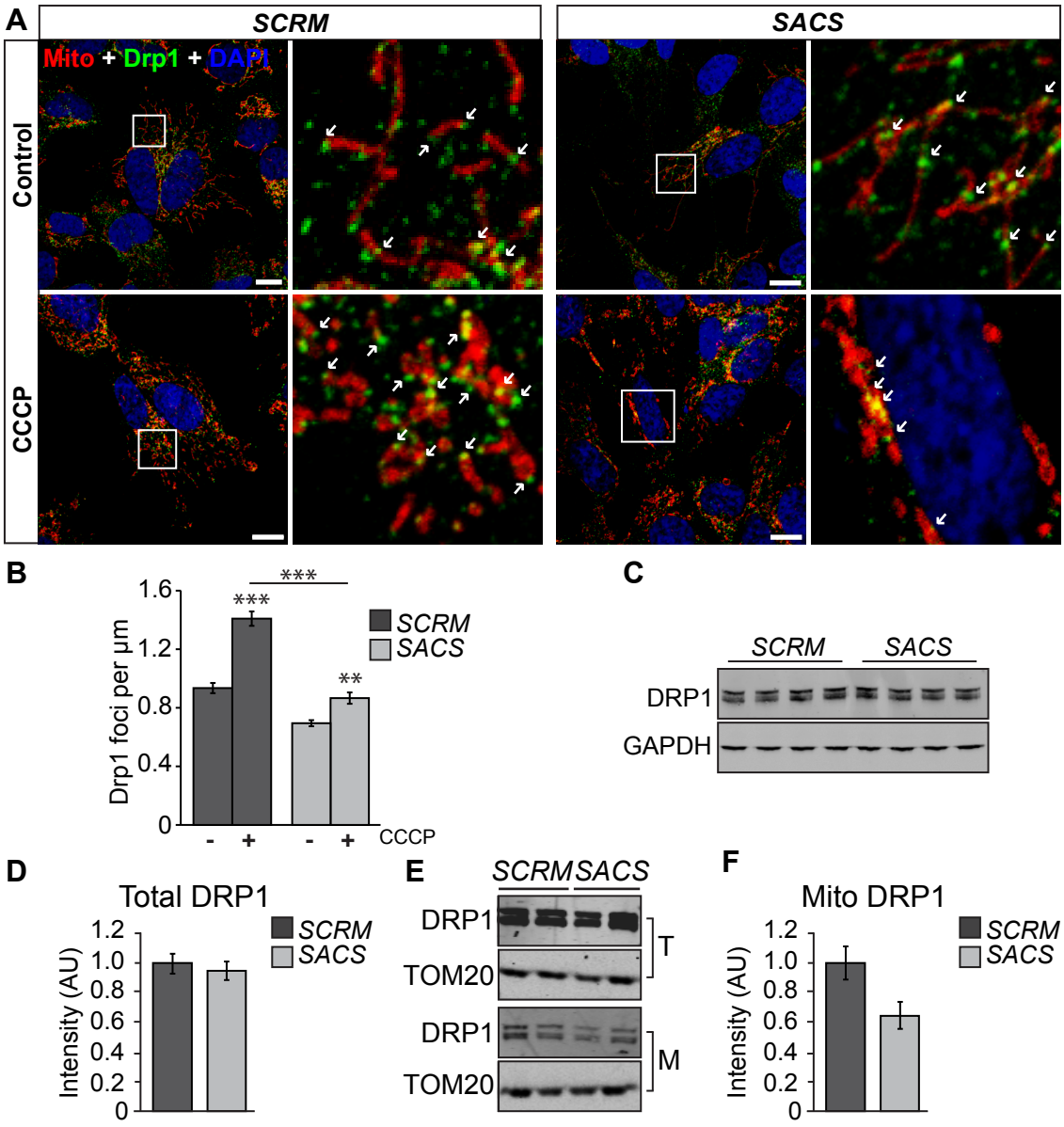

Figure S4. Localisation of Drp1 to mitochondria is reduced in sacsin knockdown SH-SY5Y cells. (A) SH-SY5Ys were cotransfected with control scrambled (SCRM) siRNA or siRNA targeting sacsin (SACS) and DSRed2-mito (red). After 48 hours cells were treated for 1 hour with CCCP and then processed for immunofluorescent detection of Drp1 (green) and counterstained with DAPI (blue) for nuclei. Examples of mitochondrial associated Drp1 foci are indicated by arrows. Scale bar = 10µm. **(B)** The number of Drp1 foci that localised to mitochondria in SCRM and SACS cells with and without CCCP treatment were then quantified from confocal Z-stacks. This data was expressed as the number of Drp1 foci localised to mitochondria per 1 µm of measured length (quantification was performed from at 14 cells per treatment, from three independent replicates). Statistical significances were determined by T test. Error bars = SEM. ** p≤0.001, *** p≤0.005. **(C)** Levels of Drp1 in SCRM and SACS cells were assessed by immunoblot, while GAPDH was used as a loading control. **(D)** Quantitative analyses by densitometry indicated that 48 hours post transfection total cellular levels of Drp1 were not significantly altered in sacsin knockdown cells. **(E)** Representative immunoblot of SH-SY5Y cells transiently transfected with *SACS* or *SCRM* siRNA and subjected to subcellular fractionation. Total (T) and mitochondrial (M) fractions were immunoblotted for Drp1 and TOM20. **(F)** Densitometric analysis of DRP1 levels in the mitochondrial fraction relative to TOM20 suggests a reduction in *SACS* compared to *SCRM* siRNA treated cells (n = 2). Error bars = SD (in D and F)

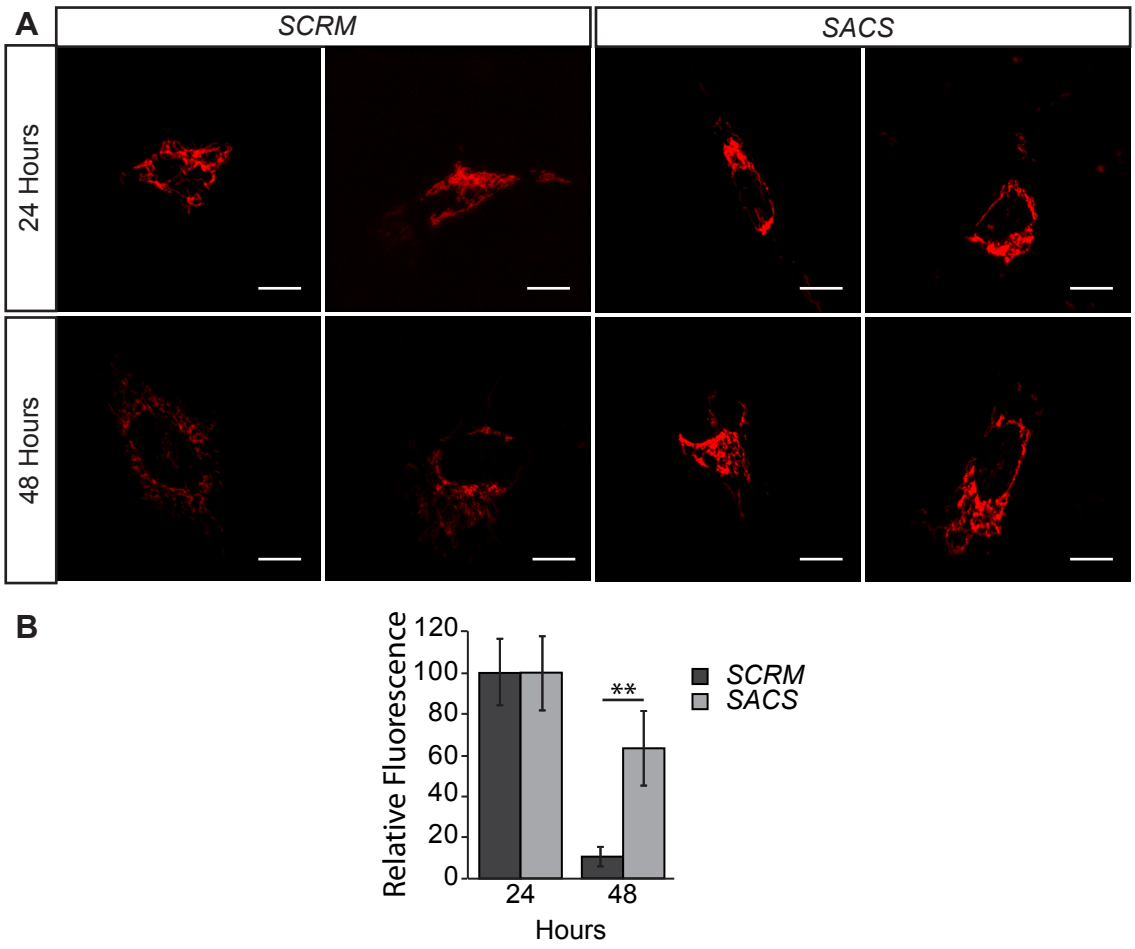

Figure S5. Mitochondrial turnover is decreased in sacsin knockdown cells. (A) Representative images of SH-SY5Y cells 24 and 48 hours after a pulse of MitoTimer protein expression. Tet-On SH-SY5Y were cotransfected with control scrambled (*SCRM*) siRNA or siRNA targeting sacsin (*SACS*) and pTRE-tight-MitoTimer (red). After 24 hours cells were treated for 1 hour with doxycycline and then returned to normal media for a further 24 or 48 hours prior to fixation and confocal imaging. **(B)** MitoTimer red fluorescent intensity was then quantified in individual cells from confocal maximum intensity projections (data is from a representative experiment, where a minimum of 9 cells was imaged per condition). MitoTimer green fluorescence was not at quantifiable levels at 48 hours post the doxacycline treatment in control or sacsin knockdown cells, consistent with a short period of MitoTimer expression, and is not shown. Error bars = SEM. ** $p \leq 0.005$.

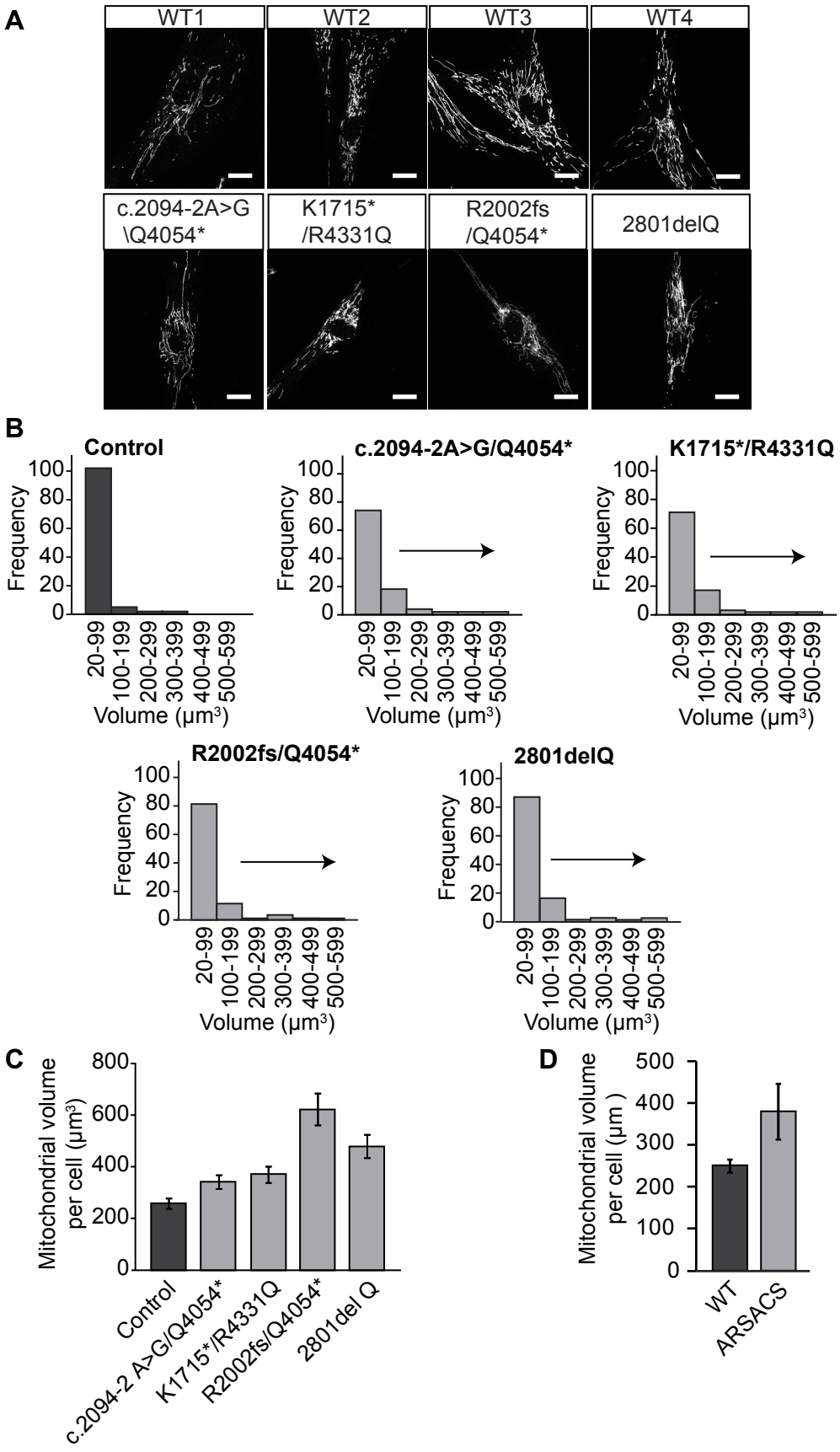

Figure S6. Mitochondrial network organisation is altered in ARSACS patient HDFS. (A) Confocal Z-stacks of live control and patient HDFs stained with MitoTraker were acquired to generate maximum intensity projections. Scale bar = 10µm **(B)** Surface rendered 3D images were generated from this data and used to calculate the number of individual mitochondria and their volume. This is shown as the frequency of individual mitochondria for a representative control cell line and each patient analysed. **(C-D)** From these data the average mitochondrial volume per cell (in μm^3) was calculated. This is shown for each patient cell line (C) and cumulative for the 4 patient cells lines analysed (D). Measurements were made in at least 25 cells per line. Error bars = SEM.

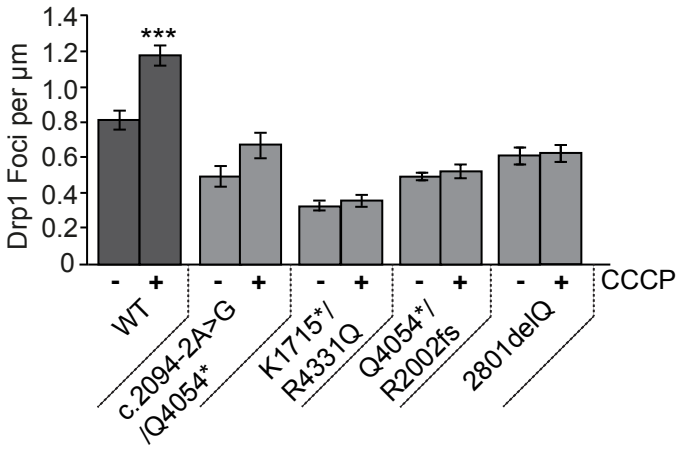

Figure S7. Localisation of Drp1 to mitochondria is reduced in all ARSACS patient cell lines. **(A)** Control and patient HDFs were treated for 1 hour with CCCP and then processed for immunofluorescent detection of mitochondria and Drp1. The number of Drp1 foci that localized to mitochondria in control and patient HDFs with and without CCCP treatment were then quantified from confocal Z-stacks. This is shown for individual patient cell lines. This data was expressed as the number of Drp1 foci localized to mitochondria per 1 µm of measured length (quantification was performed from at least 6 mitochondria in 45 cells for each treatment, from three independent replicates). Error bars = SEM. *** p≤0.005.